AD NUMBER

AD520202

CLASSIFICATION CHANGES

TO: unclassified

FROM: confidential

LIMITATION CHANGES

TO:

Approved for public release, distribution unlimited

FROM:

AUTHORITY

ONR ltr. Ser 93/804, 26 Aug 1998; Same

NORTHROP CORPORATION

LASER SYSTEMS DEPARTMENT
3401 West Broadway
Hawthorne, California 90250

SECRET

NLSD 72-7R

HIGH POWER CO LASER
SEMI ANNUAL REPORT (U)

LASER SYSTEMS DEPARTMENT
RESEARCH AND TECHNOLOGY
NORTHROP CORPORATION

March 1972

Contract No. N00014-72-C-0043

Sponsored by
ADVANCED RESEARCH PROJECTS AGENCY
ARPA ORDER NO. 1806

Monitored by
OFFICE OF NAVAL RESEARCH
CODE 421

SECRET

PROGRAM IDENTIFICATION (U)

ARPA Order No.:	1806
Program Code No.:	1E90
Name of Contractor:	Northrop Corporation
Effective date of contract:	1 August 1971 - 31 July 1972
Amount of Contract:	$537,699.00
Contract No.:	N00014-72-C-0043
Program Manager:	Dr. G. Hasserjian (213) 675-4611, Ext. 4861
Project Scientist:	Dr. M. M. Mann (213) 675-4611, Ext. 2821
Scientific Officer:	Director, Physics Program Physical Sciences Division Office of Naval Research Department of the Navy 800 North Quincy Arlington, Virginia 22217

DISCLAIMER: The views and conclusions contained in this document are those of the authors and should not be interpreted as necessarily representing the official policies, either expressed or implied, of the Advanced Research Projects Agency or the U. S. Government

HIGH POWER CO LASER
SEMI ANNUAL REPORT (U)

TABLE OF CONTENTS

1.0 SUMMARY

(S) The purpose of this program is to develop, on an approximately two year time scale, a 1 - 2 MW average power, variable pulse repetition rate diffraction-limited CO laser operating at an electrical efficiency of 50% or more. The work covered in this contract involves the design of intermediate power CO laser devices, the development of the required CO laser technology, and the construction of an intermediate power CO laser device.

(U) This program encompasses, on a best effort basis, the following major tasks:

(U) 1. The development of both steady state and transient kinetic models in order that realistic theoretical predictions of high energy device characteristics can be made.

(U) 2. Measurements of basic parameters of the CO laser at low pressures including: gain, saturation intensity, rates of vibrational cross-relaxation between CO molecules, transfer rates of CO and N_2, discharge characteristics, and spectral characteristics.

(U) 3. Measurements and characterization of a high pressure E-beam excited pulsed laser to experimentally determine transient operating parameters for high energy extraction.

(U) 4. The design and construction of a 500J/pulse diffraction-limited CO laser oscillator.

(U) 5. The development of mirror fabrication techniques for pulsed operation.

(U) 6. The development of line selection techniques for controlling the oscillator spectral output.

(S) 7. Preliminary design of a 20KJ/pulse diffraction-limited CO laser oscillator-amplifier system.

(U) The most significant accomplishments during the second quarter of this program were: the completion of the computer program for the transient analysis of the molecular kinetics of an oscillator, and the laser oscillations obtained from the E-beam stabilized discharge device operated at atmospheric pressure and room temperature. Satisfactory progress was also made in the other tasks of the program listed above. Technical reports and published papers, (see References 1, 2, 3, 4, 8, 11 and 12) contain detailed description of completed work, and a review of the highlights of the activity in the last quarter is presented here.

(U) The kinetic model for CO and N_2 gas mixtures was extended from a cw to the transient analysis of both oscillators and amplifiers. Numerical results from the model were compared with the experimental laser data from the E-beam stabilized device. These comparisons, even though limited in number, show excellent agreement. Parametric investigations with the analytic model were also made. These investigations indicate two significant laser characteristics that were not initially recognized. The model indicates that high electrical pumping rates ($\sim$20 kW/cc) are required to achieve early onset of lasing ($\lesssim$10 μs), and high efficiency. Also, with high pumping rates and low temperature operation, the laser emission may be controlled to occur in the lower vibrational bands. A number of rotational transitions in the vibrational bands 6 - 5 and lower have excellent propagation characteristics in the lower atmosphere. This brings out the possibility of achieving a certain degree of line selection by controlling the kinetics

of the laser gas. Some of these results are reviewed in the next section.

(U) Measurements of small signal gain in low pressure lasers were completed, and a set-up is ready for measurements of gain with the E-beam stabilized device. A three laser experimental set-up was completed to measure vibrational cross-relaxation rates. However, initial data are not conclusive due to the sensitivity of the present set-up to mechanical vibrations. More definitive data are anticipated during the next quarter.

(U) Extensive measurements were made with the E-beam stabilized discharge laser at room temperature. These measurements included both tests of discharge characteristics and laser measurements with stable cavity configurations. Attempts at low temperature operation were not successful with the original set-up due to large temperature gradients that existed with the static gas conditioning system. Average gradients have been eliminated with a flowing system, but problems with optical scintillation due to random thermal inhomogeneities have restricted experiments at high pressures. The new experimental system is described in Section 3.0 in addition to the experimental data.

(U) The design effort of the 500J/pulse diffraction-limited laser oscillator was concentrated on the resonator configuration capable of achieving mode quality as well as line selection. A compound resonator configuration has been designed which can accommodate line selection elements. Section 4.0 contains a review of this design. A water vapor cell, with components for control of vapor pressure and temperature, has been constructed and is being tested for characterization as a line selective component for the resonator of the laser oscillator.

(U) The feasibility of fabricating post-mounted substrate mirrors was demonstrated during the first quarter of this program. Surface polishing and coating techniques have been developed for two copper alloys, Berylco 10 and 25, and mirrors with these alloys have been fabricated for the experimental lasers of this program. In addition, a computer program of the analytical model of post-mounted mirror substrates has been completed that can provide design parameters of low distortion mirrors under loaded conditions. A review of these results, faceplate fabrication techniques and the description of apparatus for testing mirror distortion is given in the last section.

2.0 THE KINETIC MODEL AND TRANSIENT ANALYSIS

(U) Significant progress has been made in analytical modeling of the electrically excited CO laser under various operating conditions. This model has been verified by comparison with experimental measurements of small signal gains in low pressure cw amplifiers. In addition, the transient analysis provided by the model has been compared with preliminary results of data for a high pressure, E-beam stabilized, CO laser oscillator. In this section, a review of the model is presented and performance predictions for a variety of high pressure pulsed systems are discussed.

2.1 Theoretical Description. (U) In order to obtain a theoretical understanding of the electrically excited CO laser, a molecular kinetic model and computer code have been developed for either a cw or transient analysis of an oscillator or amplifier. The goal of this effort is to provide a reliable model for guiding the design, and for predicting the radiative characteristics, of high power pulsed and cw CO lasers. Although a completely self-consistent analysis should attempt to treat both the molecular and plasma kinetics on an equal basis as a coupled system, there is much useful information that can be obtained by analyzing them independently. The basic reason for this is that the characteristics of one system are reflected somewhat insensitively in the resulting properties of the other. The detailed structure of the electron energy distribution does not critically effect the integrations over the excitation cross sections that give the rates for electron pumping of the molecular vibrational levels. Thus, even though the electron energy distribution function may display very important behavior in the energy regions of interest for vibrational excitation, use of a (incorrect) Boltzmann distribution can give approximately the correct rates if the electron temperature and density are

chosen properly. Future efforts will be made to extend the present molecular kinetic analysis to include plasma kinetics properly. More complete details of the present model, applied to low pressure cw amplifier calculations, have been described elsewhere[1, 2, 3] and preliminary results of calculations for high pressure transient CO oscillators have recently been reported.[4]

(U) The molecular kinetic model and computer program have been developed for electrically excited (CO, N_2, He, Ar, ...) gas mixtures, with up to 50 levels for CO and 30 for N_2. The population distributions n_r and N_R of the CO and N_2 vibrational levels are determined by a variety of competing pumping and relaxation processes, and satisfy the master equation,

$$dn_r/dt = R_r^e + \sum_x R_r^{VT}(CO^+, X) + R_r^{VVT}(CO^+, CO^+) + R_r^{VVT}(CO^+, N_2^+) + R_r^{spon} + R_r^{stim} + R_r^{misc}$$

$$dN_R/dt = R_R^e + \sum_x R_R^{VT}(N_2^+, X) + R_R^{VVT}(N_2^+, N_2^+) + R_R^{VVT}(N_2^+, CO^+) + R_R^{misc}$$

In the steady state, the time derivatives are set equal to zero, and the equation is volved algebraically using a generalization of the Newton-Raphson technique for a system of simultaneous nonlinear equations. For a transient analysis, the equations are numerically integrated. In the order of their occurrence, the pumping and relaxation processes of this equation include:

(1) Electron impact excitation of CO (and N_2),

(2) VT deactivation collisions,

(3) VV (near-resonant, single quantum) exchange collisions,

(4) Spontaneous decay ($\Delta v = 1, 2$),

(5) Stimulated emission and absorption processes for P(J) lines,

(6) Miscellaneous pumping or decay terms,

and are given by:

$$R_r^e = -n_r \sum_s R^e_{r\to s} + \sum_s n_s R^e_{s\to r}$$

$$= n_e \sum_s \left[n_s - n_r \exp\left(\frac{E_r - E_s}{kT_e}\right)\right] \langle v(E)\, \sigma_{s\to r}(E) \rangle_{T_e}.$$

$$R_r^{VT}(CO^+, X) = [P^{VT}_{r+1\to r}(CO, X)\, n_{r+1} - P^{VT}_{r\to r+1}(CO, X) n_r$$

$$- P^{VT}_{r\to r-1}(CO, X)\, n_r + P^{VT}_{r-1\to r}(CO, X)\, n_{r-1}]\, n^X$$

$$R_r^{VVT}(CO^+, CO^+) = \sum_s [P^{VVT}_{r+1,\, s-1\to r,\, s}(CO, CO) n_{r+1}\, n_{s-1}$$

$$- P^{VVT}_{r,\, s\to r+1,\, s-1}(CO, CO) n_r n_s + P^{VVT}_{r-1,\, s+1\to rs}(CO, CO) n_{r-1} n_{s+1}$$

$$- P^{VVT}_{r,\, s\to r-1,\, s+1}(CO, CO) n_r n_s]$$

$$R_r^{VVT}(CO^+, N_2^+) = \sum_R [P^{VVT}_{r+1,R-1 \to r,R}(CO, N_2) n_{r+1} N_{R-1}$$

$$- P^{VVT}_{r,R \to r+1,R-1}(CO, N_2) n_r N_R + P^{VVT}_{r-1,R+1 \to r,R}(CO, N_2) n_{r-1} N_{R+1}$$

$$- P^{VVT}_{r,R \to r-1,R+1}(CO, N_2) n_r N_R]$$

$$R_r^{spon} = -n_r(A_{r \to r-1} + A_{r \to r-2}) + n_{r+2} A_{r+2 \to r} + n_{r+1} A_{r+1 \to r}$$

$$R_r^{stim} = - n_r S_{r \to r-1} + n_{r-1} S_{r-1 \to r} - n_r S_{r \to r+1} + n_{r+1} S_{r+1 \to r}$$

where

$$S_{r \to r-1} = I(\nu_{r,J}) \sigma_{r \to r-1}(J)/h\nu_{r,J} .$$

For a detailed discussion of the assumptions and the theories of rates used in this model, the earlier references (2, 3) should be consulted.

(U) In the case of an amplifier analysis, the intensities $I(\nu_{r,J})$ that occur in the rates for stimulated emission and absorption are external inputs. For the case of an oscillator, radiation intensities are calculated in a completely self-consistent way by requiring that the gain coefficients α of the oscillating transitions must be instantaneously equal to the loss coefficients. These intensities must be such that the rates of stimulated emission, in combination with the rates of all the other kinetic processes present, shall produce temporal changes in the evolution of the population distribution that maintains this condition. It is assumed that rotational cross-

relaxation is fast enough that only one rotational line - the P(J) transition highest above (or at) threshold - can oscillate in any given vibrational band. The rotational levels are assumed to be in thermal equilibrium characterized by a temperature T_{rot} which need not be taken equal to the molecular kinetic temperature T_{mol}. Losses, such as mirror absorption, output coupling, Brewster window loss, etc. are assumed to be uniformly distributed throughout the laser gain medium. (These cavity losses are assumed to be small enough that the assumption of a spatially uniform intensity distribution in the active medium is adequate to describe the molecular kinetics and radiative characteristics.) Selective losses can be entered as inputs to the program, thus permitting the analysis of a line-selected oscillator. From the threshold condition $R\exp 2(\alpha - \gamma) L = 1$, the gain coefficient for an oscillating line must be given by $\alpha = \gamma + (1 - R)/2L$, where γ is the loss per pass exclusive of the output mirror. The losses in the output mirror are included in γ, so that the output coupling is given by $T/2$, where T is the mirror transmission.

(U) The computer program calculates vibrational population and temperature distributions, gains, saturation characteristics, energy transfer and extraction rates, conversion efficiencies, output intensities, and spectral identification as a function of time. These quantities are all required for a complete description of the laser system, and the detailed information is necessary for determining the optimum operating parameters for achieving a variety of objectives. The optical extraction for a CO laser system is characterized by several different efficiencies, all of which must be combined to obtain an estimate of the overall efficiency. The ultimate attainable extraction efficiency for a CO oscillator is limited by the following factors:

(1) Quantum efficiency

(2) Electrical excitation efficiency

(3) Output coupling efficiency

(4) Line selection efficiency

(5) Volumetric extraction efficiency

(6) Pulse length limitations

(U) The "quantum efficiency," which is primarily a property of the molecular kinetic processes, is the fraction of vibrational excitation that goes into stimulated emission, rather than into heating losses, diffusion losses, spontaneous fluorescence, or (in the case of pulsed operation) establishment of the vibrational distribution. Since CO is a diatomic molecule with only one ladder of energy levels, and since VT collisional processes and spontaneous emission are relatively slow, it is possible to obtain quantum efficiencies approaching 100%. The lower laser level of a given transition can serve as the upper level of a subsequent transitions, thus permitting vibrational energy to be extracted as coherent radiation through several pairs of levels for which the populations are sufficiently inverted. As a result of the rapid redistribution of electrical excitation energy among the vibrational levels by means of the near-resonant VV exchange collisions, a molecule reaching a terminal laser level can be reexcited, and thus the absence of lasing on the lowest levels need not severely limit the efficiency. The VV heating resulting from the anharmonicity of the vibrational energy levels is one of the primary loss mechanisms that limits the quantum efficiency (typically ~90%).

(U) The electrical excitation efficiency is the fraction of electrical input energy transferred to vibrational energy, rather than to other processes, (e. g. electronic state or ionization excitation or collisional plasma heating),

and is basically a characteristic of the plasma kinetics. The role of the various gas constituents, operating parameters, and electrical excitation techniques that can be employed to optimize the plasma characteristics to attain high electrical transfer efficiencies are now reasonably well understood. Nighan[5] has shown that, with suitable adjustments of the plasma E/N, it is possible to obtain electrical excitation efficiencies approaching 100% in CO, N_2 discharges.

(U) The quantum efficiency characterizes the total radiative conversion of vibrational energy in the active medium for an oscillator with an optical loss per pass of (γ + T/2). The fraction of that amount that can be extracted as output is given in the present approximation by the coupling efficiency $(T/2)/(\gamma + T/2)$. Clearly, in order to maximize this quantity, the output coupling loss for the oscillator must be large compared to all the other optical losses in the cavity. However, choice of coupling loss must also be determined by other factors, such as laser turn-on time in a pulsed system.

(U) The volumetric extraction efficiency is simply the fractional part of the gas volume which contributes to output radiation. The spectral limitation imposed by line selection will also limit the quantum efficiency to a value less than that which would be obtained in a free-running oscillator. (Depending upon the precise technique of line selection employed, there may also be degradation of the output coupling efficiency.) For pulsed operation, the laser turn-on time depends primarily upon the rates of electrical excitation per unit volume, the partial pressures of the gas

constituents, and the total optical loss/pass in the cavity. Thus, if short pulse operation is required, the ultimate attainable energy efficiency will depend sensitively upon the time necessary to reach threshold, and upon the time to approach steady state.

2.2 Results of Parametric Calculations. (U) A variety of calculations have been carried out for different parametric cases, with some of the results summarized in Table I. Because of the importance of attaining adequate electrical excitation, the total input power per unit volume transferred to vibrations is included in the data presented. Although detailed results of spectral characteristics for all of these cases is not possible here, calculations have shown that the relative effects of electrical pumping and VV cross-relaxation can produce significant effects, both qualitative and quantitative, on the output spectrum. The onset of lasing is determined primarily by the total optical losses in the cavity and the electrical excitation rate; these times are also summarized in Table I for each of the cases.

(U) In Figure 1, 2, and 3, the percentages of electrical input power that goes into optical extraction, kinetic heating, and establishment of the vibrational distribution is shown plotted as a function of time for three cases listed in the Table, in which the electrical input rate has been varied. An earlier time for attainment of threshold is illustrated by Figure 3, for which the electrical pumping rate is highest. The dotted extension of the curves in Figure 1 shows the case for which there is no lasing permitted.

(U) In Figure 4, similar curves are constructed to compare two extreme examples of electrical pumping rate versus VV cross-relaxation. In (a), the gas mixture is CO/N_2 = 50/300 torr, with electrical input of

16.6 - 12.0 kW/cm^3, while in (b), the gas mixture is CO/N_2 = 250/500 torr, with an input power of 2.7 - 1.9 kW/cm^3. (Input powers refer to the beginning and end of the pulse; for a Boltzmann with n_e and T_e assumed to be fixed, electrical excitation must decrease as the vibrational distribution is established.) The output spectra at 300 μ sec for the two cases displayed in Figure 4 are compared in the insets to that Figure. (The relative intensity scale for (a) is ten times that for (b) in these insets). The effect of the significantly higher ratio of electrical to VV pumping for case (a) is dramatically reflected in the output characteristics, as well as in the time dependence of the optical extraction efficiency.

(U) An illustration of the effects of line selection limitations on the output efficiency is shown in Figure 5, 6 and 7. In all of these cases, the gax mixture consisted of CO/N_2 = 100/650 torr, with an initial power input of ~23.4 kW/cm^3 ($n_e = 10^{12}$/cm^3, T_e = 8000°K). The molecular and rotational temperatures were assumed to be 125°K, the cavity length was 1 m, and the output mirror was assumed to have 90% reflectivity. No other cavity losses were assumed for the oscillating transitions, so the output coupling efficiency for all of these cases was 100%. The inset to Figure 5 shows the output spectrum at t = 100 μsec for the free-running oscillator, which attains a steady state quantum power efficiency of ~90%. In Figure 6 and 7, the effects of line selection are illustrated. In the case of Figure 7, it was assumed that an infinite loss on all lines except 1 → 0 P(11), 2 → 1 P(15), 3 → 2 P(16), 4 → 3 P(15), 5 → 4 P(15), and 6 → 5 P(10) (i.e., those with the best atmospheric transmission characteristics) was introduced into the cavity. In Figure 6 a case of less stringent line selection is illustrated. This calculation assumed infinite loss for all lines except those P(J) transitions in bands from 1 → 0 to 6 → 5 having inverse atmospheric attenuation coefficients greater than or equal to 10 km. The cases illustrated in Figure 5 and Figure 7

were also restarted at t = 100 μsec, and run for an additional 50μsec with the electrical excitation turned off, in order to estimate the energy efficiencies for a realistic pulse duration, with and without line selection. A comparison of the total energy efficiency of these two cases shows that the line selected case has a pulsed energy efficiency of 52% and the unselected case has an efficiency of 74%. Therefore, the more restrictive line selection results in a 30% degradation of the quantum efficiency.

3.0 EXPERIMENTS WITH AN E-BEAM STABILIZED DISCHARGE LASER

(U) In the previous quarterly report, the experimental E-beam stabilized discharge device was described. In that period, the laser gas conditioning system was a static one. The temperature conditioning was accomplished by a low temperature bath enveloping the laser plenum chamber. This system did not provide adequate thermal uniformity in the discharge region causing large density gradients. The system has since been converted to a flow system to maintain uniform gas in the discharge volume at low temperatures. The experimental device, flow system and operating conditions are reviewed below. Adequate medium homogeneity has been accomplished either at high temperatures and pressures near static conditions or at low temperature and at reduced pressures at high flow rates. The system is being improved to achieve low temperature-high pressure operation. Some typical experimental data are presented in the next section, and compared with calculations of the analytical model which show excellent agreement.

3.1 The Experimental Device for High Pressure Pulsed Measurements. (U)

To verify the predictions of the transient model and to obtain initial engineering experience for construction of large high power pulsed CO devices, the relatively small (nominally 1 liter) E-beam stabilized transverse discharge laser was constructed. This device, which is now being used to perform parametric studies and diagnostic measurements for pulsed operation of CO/N_2 mixtures, is basically similar to those used for high energy CO_2 lasers,[6,7] and is shown schematically in Figure 8. However, the design is somewhat more complex in order to satisfy the requirement of low temperature operation.

(U) As described in our first quarterly report, the electron gun was built by Physics International and extensively modified by Northrop. It

was designed to supply a current density of 1.0 mA/cm^2 through an output aperture of 3 cm x 100 cm. The pulse duration can be varied from 20 to 500 μsec. The nominal accelerating voltage is 165 kV. The sustainer supply consists of a 50 kV, 40 μf capacitor bank with a crowbar which can be activated in case of fault or at the end of the gun pulse.

(U) One of the most difficult engineering problems encountered with high pressure operation of the laser was the maintenance of adequate medium uniformity at cryogenic operating temperatures. The severity of the problem may be appreciated by noting that for a CO/N_2 mixture at 100°K, a transverse gradient of only 1°C/cm will produce one milliradian of beam steering in the present device. Random fluctuations in temperature of this order will also produce excessive scintillation. Therefore, it is necessary to maintain the gas temperature uniform to within a small fraction of a degree. The nature of the boundaries made it difficult to maintain this type of uniformity in our initial static system; the experimental device now employs a flowing system.

(U) The flow direction is from anode to cathode to permit the use of temperature controlled boundaries on three sides of the discharge region, and to minimize the extent of the cathode boundary layer. The sustainer electrodes are both porous. The cathode has an optical transmission of 55%, and the anode structure has a dense sintered wire mesh screen on the discharge side of its surface. Flow is introduced through the anode and extracted through two narrow manifolds between the cathode and gun.

(U) The flow system can provide mixtures of CO (or CO_2), N_2, He, and Ar gas at flow rates up to 100 SCFM. The operating pressure is controlled between 100-760 torr by a vacuum controller and 300 CFM

vacuum pump. The gas is cooled by a liquid nitrogen heat exchanger, and final temperature conditioning is provided in the cooled anode assembly. Vacuum insulated internal CaF_2 windows are employed to minimize heat leaks at the optical boundaries. To date, the problem of controlling medium homogeneity at cryogenic temperatures has limited laser experiments to near ambient temperatures. Typical results are presented in the next section. Temperature conditioning systems of both the gas and the laser plenum are being modified to obtain a uniform medium at temperatures near 100°K.

(U) Discharge measurements with various gas mixtures and pressures were also made to investigate discharge stability and plasma parameters. CO laser discharges are generally quite stable due, in part, to the absence of noble gases in the mixtures. Stable pulses of more than 300 μs duration could be obtained with sustainer fields of 5 kV/cm. The measured discharge characteristics agree favorably with analytical predictions. A typical comparison is presented in Figure 9. 1 This work will be presented in greater detail elsewhere.[8]

(U) The maximum electrical pumping that is attainable with the present 0.5 mA/cm^2 electron beam is 4 kW/cc. The requirements of the analytical model for efficient operation of a high power CO laser show that at least 20 fold increase in E-beam current density is required to achieve the high pumping rate of approximately 20 kW/cc. For this reason, a gun is being designed which will be capable of delivering up to 100 mA/cm^2.

3.2 Comparison of Kinetic Modeling Calculations with Experiment. (U) Experimental measurements have been made of small signal gain coefficients in a low-pressure cw amplifier, and these values were fitted numerically to the gain equation, using a least squares technique, to obtain the vibrational populations and rotational temperature.[1] The present

kinetic model produced good agreement with experimental population densities, using physically realistic choices of values for the various rate constants (most of which were taken from independent sources). Figure 10 shows this comparison, with the experimental data indicated by solid circles. Experimental data and model parameters for this calculation are summarized in the inset.

(U) The predictions of the theoretical model are also in agreement with the results of experiments with the E-beam stabilized discharge, high pressure CO laser measurements. Results for a case at high pressure and near room temperature are shown in the inset of Figure 11. The upper trace in the oscilloscope photograph shows the detector output, which is reproduced by the dotted curve in the enlargement of that Figure. Threshold occurs 200 μsec after the initiation of the pumping pulse, and oscillation continues well after the termination of the excitation at 300 μsec. The experimental data is compared in Figure 11 with the results of theoretical predictions, indicated by the solid curve. Parameters assumed for the model calculations are also summarized in the Figure. The values used for n_e, the electron density, and T_e, the electron temperature, were consistent with independent plasma calculations[8] and with Nighan's[5] calculations of average electron energy as a function of E/N, and were chosen in such a way as to give the correct (experimental) value for the electrical excitation power per unit volume. The theoretical model predicts a total optical output energy extraction of 1.2J/liter during the excitation period, with an additional output of 4.8J/liter in the following 300 μsec. Electrical excitation input energy was calculated to be 360 J/liter, giving a volumetric extraction efficiency (over the 600 μsec duration) of ~1.5%. Similar calculations were carried out for a variety of different parametric assumptions. Probably the most important uncertainty in comparing theory with experiment is the assumed parameter for output coupling loss and total optical loss in the

cavity. The cases in which these quantities were varied by factors of ~2 produced changes in output of only a factor of ~4, and laser turn-on time change of ~10%. Similar results were obtained at lower pressures and temperatures. More detailed parametric data, both experimental and analytical will be given in the next quarterly report.

4.0 RESONATOR DESIGN FOR DIFFRACTION LIMITED AND LINE SELECTED OPERATION

(U) During the last quarter, a great deal of emphasis was placed on developing a resonator design for diffraction-limited operation along with the line selection requirements for the CO laser oscillator. In the previous quarterly report, a brief review of the compound resonator configuration was given, the design of which is being developed to meet the above requirements. In the sections below a more detailed description of the resonator is presented with recent design data for beam profile control. Line selection requirements are discussed in view of the more recent kinetic calculations of spectral characteristics of high pressure CO lasers. Also, the design and testing effort of a water vapor cell as a line selection element is described.

4.1 The Resonator Design and Output Beam Profile. (U) A resonator configuration has been designed to give good mode properties and to be compatible with the planned line selection techniques. The mode properties and emission frequencies are determined by a low Fresnel number oscillator located coaxially at the center of a high Fresnel number amplifier as shown in Figure 12. The oscillator output is injected into the outer amplifier region; thus the output should have the desirable mode quality and stability of a low Fresnel number oscillator, and line selection can then be accomplished on the physically smaller beam. It is anticipated that the small-signal gain in the amplifier will be sufficiently high so that only one round trip will be required to efficiently extract the energy from this region.

(U) The resonator configuration described above has the additional advantage that it can be modeled analytically. Since the amplifier Fresnel number is very large and there is no feedback, the transit through this region can be described using geometrical optics. The major effects of interest, then, are those generated by the mirrors (primarily radii of

of curvature variations and misalignment) and those generated by the laser medium (gain variations, including saturation, and refractive index gradients). The oscillator has a small Fresnel number and can thus be analyzed including the effects of diffraction, by numerically integrating the Fresnel-Kirchhoff equation.

(U) A computer code has been generated for the primary purpose of analyzing the mode structure of the oscillator for a variety of resonator configurations. Lumped gain elements have been included on each mirror with phenomonological gain saturation but without diffraction in the elements. The primary resonator configurations that have been studied are confocal, unstable resonators with a variety of mirror g-parameters and cavity Fresnel numbers. The analytical results show that it is possible to decrease the peak mirror loading and tailor the beam shape injected into the amplifier region by controlling these resonator parameters.

(U) The computer code is cylindrically symmetric, iterative program similar to that used by Fox and Li,[9] where an initial amplitude (usually uniform) is assumed on one mirror and the resulting amplitude at the opposite mirror is computed. This amplitude is then used as the source for computing the amplitude back at the first mirror. The process is repeated until the steady-state mode profile is obtained. Intensity and phase profiles are printed on each transit so the time required for stabilization is also obtained.

(U) A number of programs were run to investigate the effects of gain saturation on the mode profile. The extent of this effect depends upon the level of saturation, i.e., the output coupling coefficient. However, at intensities well above saturation the principal effect is that the intensity

profile is generally flattened somewhat and the ring structure corresponding to the Fresnel zones is enhanced. The profile flattening occurs because the gain is maximum where the intensity is minimum. This, in turn, is expected to enhance the bright and dark intensity ring structure toward that expected from the near-field pattern of a uniformly illuminated aperture. Since the profiles do not change drastically, most of the parametric studies were performed without gain and the results, therefore, reflect only the effects of changes in the resonator parameters.

(U) The phase versus radius profiles for all of the confocal unstable resonators studied were uniform to less than ± 20 degrees over 90% of the resonator radius. In contrast to this, the intensity versus radius profiles at the mirrors vary considerably with changes in the resonator parameters. By choosing the proper resonator parameters an intensity profile can be selected to reduce the peak mirror loading, and to generate almost any desired output profile for injection into the amplifier.

(U) The Fresnel number $(a_2^2/L\lambda)$ based on the radius, a_2, of the large mirror is extremely important in determining the intensity profile at the output mirror. In general, if this Fresnel number is chosen to be even, then the intensity will decrease at the beam center, and if it is odd, the intensity will peak at the beam center. This occurs because the illumination from the large mirror, although not uniform, has nearly planar phase fronts. Thus the shape has the same qualitative features of an aperture illuminated by a uniform plane wave, although the peaks and minima are not as strong. These features can be utilized to minimize the peak mirror loading as is illustrated in Figures 13 and 14. The resonator for Figure 13 was chosen to have a Fresnel number FN = 6.0 based on the large mirror, and results in a dip at the beam center on the small mirror. Simultaneously, the Fresnel number based on the small mirror radius (a_1) including the

curvature of the phase front (called FN_{eff}) is chosen to be 2.0 which, as expected, results in an intensity dip at the center of the large mirror. For a given output coupling coefficient δ, the peak intensity will, in general, decrease as the radius of the peak position is increased. The opposite case is illustrated in Figure 14 where both FN and FN_{eff} are chosen to be odd. As expected, the intensity profiles on both mirrors peak at the beam center, maximizing the peak mirror loading.

(U) The wide range of possible output intensity profiles which can be achieved is illustrated for two cases in Figure 15. The first profile has an intense peak at the center and an output which is uniform over much of the coupling region ($r > a_1$). In contrast to this the second profile is highly tapered over the coupling region. This range of shapes can be utilized to compensate for variations in the gain profile (due to nonuniform pumping or gain saturation) in order to get the desired profile out of the amplifier, e.g., a nearly uniform profile. It is interesting to note that in the second case the peak output intensity occurs completely off the mirror surface.

(U) The laser medium itself, because of the length, gain, etc., may dictate some of the resonator parameters so that complete freedom in choosing the parameters is not usually possible. For example, the magnification (M) must be consistent with the small-signal gain, or lasing action will not even occur. However, with the constraints, small variations in the parameters may, as shown above, change the mode considerably and they must be chosen carefully.

(U) A resonator configuration suitable for the inner oscillator of a high gain laser has been designed and the optics have been fabricated. These will be tested on the current high pressure pulsed CO laser.

4.2 Predictions for Line Selection Requirements. (U) The information currently available on the atmospheric absorption of carbon monoxide laser emissions[10] covers only spectral lines attainable with a low pressure dc discharge CO oscillator. A computer model was completed (similar to that described in reference 10) in order to investigate the propagation characteristics of the predicted spectral lines emitted from a high pressure E-beam pulsed discharge. Table II lists the lines having theoretical E-folding distances of 10 km or better as predicted by this model for a 1 km atmospheric path at sea level using the Midlatitude Winter Model of reference 10. Figure 16 illustrates the absorptance/transmittance of all lines from 1900 cm^{-1} to 2140 cm^{-1} resulting from the above calculations. The calculations were made considering only water vapor absorption which is the predominant absorber in this spectral region. There may be some contribution on the high frequency end due to carbon dioxide and ozone but these effects could not be included at this time because of the unavailability of appropriate data for these atmospheric constituents. Since it is undesirable to have laser emission at spectral frequencies which will not significantly propagate in the atmosphere, the results of this study show that an efficient high power laser oscillator should have an operating spectral bandwidth of from about 1970 cm^{-1} to 2140 cm^{-1}. In addition it is necessary to reject lines in this region which do not have high transmission through the atmosphere.

(U) Kinetic calculations of high pressure, low temperature, pulsed discharge lasers indicate that it is possible to control the CO laser emissions to the lower vibrational band transitions. This effect is pointed out in the results of Section 2.2. At low temperature operation and at electrical pumping rates higher than 20 kW/cc most of the oscillator output energy is due to the transitions in the vibrational bands $6 \rightarrow 5$ and lower. From Table II it can be seen that there are numerous rotational lines in this region which have an

e-folding distance of more than 10 kms. The goal of the present effort is therefore to achieve vibrational band selection by controlling the kinetics as much as possible, achieve rotational line selection by the water vapor cell reviewed in the next section, and in addition, identify the design of feasible band pass optical components for the resonator.

4.3 The Design and Testing of the Water Vapor Cell. (U) The preliminary results obtained by this department and reported elsewhere[11, 12] indicate that line selection of a low pressure longitudinal discharge laser can be accomplished using a water vapor absorption cell internal to the laser resonator. In these experiments a 70 cm cell at atmospheric pressure was placed in a laser cavity and the temperature of the saturated water vapor was varied between 20°C and 100°C. Figure 17 shows typical spectral outputs for vapor pressures corresponding to water temperatures of 20°C and 70°C, illustrating the shifts in the rotational lines. Net single-pass gains computed from extrapolations of experimental gain data and the calculated water vapor absorption coefficients at 85°C, are shown in Figure 18 for vibrational bands 7→6 and 6→5. In the 6→5 band the emission at 20°C vapor pressure is on the P(12) line which has the highest net gain, but shifts to P(10) which has the highest net gain when the water cell temperature is elevated. The results for the transition 7→6 are similar, as laser emission shifts from P(12) to P(9). It should be emphasized that these are calculated gain data; perturbations of the population densities in one band caused by lasing in other bands have not been included, but the results are qualitatively as expected.

(U) Based on the above preliminary results, an absorption cell system was designed and constructed, to verify, in more careful and detailed experiments the theoretical absorption coefficients of the CO spectral lines, and to use as the line selection device in high pressure E-beam pulsed lasers. The present system is illustrated in Figure 19. The actual

vapor cell is constructed of stainless steel with a high temperature ceramic interior coating. It has a 2.5 cm diameter clear aperture and an optical path length of 71 cm, and has two CaF_2 Brewster angle windows. The cell temperature can be varied from 25°C to 200°C. The cell pressure can be varied from 0.01 torr to in excess of 5 atmospheres. The system can provide water vapor up to 2 atmospheres, and has provisions for introducing additional absorbing or broadening gases up to a total pressure of 5 atmospheres. The basic cell will be used in conjunction with the high pressure laser oscillator tests, with minor changes in the peripheral equipment.

(U) The experimental layout for measuring the absorption coefficients and for calibrating the cell is illustrated in Figure 20. The set-up consists of two consecutive resonator configurations with a common, low pressure CO laser gain medium. One resonator has the vapor cell and the other has a Brewster plate as a calibrated attenuator. Q-switched single line operation is achieved with a rotating mirror and a diffraction grating, giving two pulses for every rotation of the mirror. One pulse occurs when the resonator with the rotatable Brewster plate is aligned and the other pulse occurs when the resonator with the absorption cell is aligned. With the cell evacuated and the Brewster plate at Brewster's angle, the two pulses are equal in amplitude and shape. When water vapor at a particular temperature and pressure is admitted to the cell, the second pulse will decrease in intensity due to the absorptive loss introduced. The Brewster plate is rotated to introduce an equivalent reflective loss so that the first pulse has the same intensity as the second pulse. The amount of loss introduced by the cell is determined from the calibrated loss curve of a Brewster plate as a function of its angle.

(U) Detailed measurements are now being made to calibrate the cell and correlate the results of measurements with the theoretical predictions of the computer model. The self-broadening effect of water vapor is significant in this cell at high pressure and thus can not simply be extrapolated from atmospheric studies.

(U) Initial results have been obtained for two spectral lines for one set of water vapor parameters. Figure 21 shows the actual pulses obtained for the 10 - 9 P(14) line. These are the pulses viewed by a In:Sb detector at the output of a spectrometer. The output pulse is not totally comprised of a single frequency as illustrated by Figure 22; there are low level contributions from the 11 - 10P(8) and 11 - 10P(9) lines which account for the instability seen in the total output pulse. The time scale in these figures is 1 μsec/div. Figure 21a shows a multiple sweep exposure of the two pulses in the calibration mode: the absorption cell is evacuated and the Brewster plate is at Brewster's angle. Figure 21b shows these two pulses when 188 torr of water vapor at 68^{o}C is contained in the cell and the Brewster plate is at Brewster's angle. Note the decrease in energy of the cell pulse. Figure 21c shows both pulses after the Brewster plate has been tuned to insert an equivalent amount of loss in the reference resonator.

(U) The table below shows the results of measurements for two CO laser lines analyzed and compared with the theoretical predictions. The initial results indicate that the actual absorptive loss of water vapor in a confined cell for CO laser radiation may be higher than theoretically predicted. The self-broadening effects may be larger than investigators have estimated and/or the tails of adjoining absorption lines may be more significant than previously noted. Extensive data will be taken and analyzed for all possible CO laser lines and for various water vapor parameters.

Spectral ID	ν (cm^{-1})	Absorptance	
		Theoretical	Experimental
9 - 8P(14)	1854.927	0.0243	0.0520
10 - 9P(14)	1880.330	0.0238	0.0745

(U) As the above experiments are being conducted, the absorption cell system is being tested in order to determine and resolve any engineering problems so that the basic system will be compatible with the high power E-beam excited devices. The water vapor cell should give the rotational line selection desired but vibrational band selection will also be required. Band limited reflective coatings for the resonator mirrors are presently being designed and developed, in addition to considering vibrational band selection with the control of the kinetics. Alternate approaches of line selection are also being investigated.

5.0 PULSED MIRROR DEVELOPMENT

(U) A moderate amount of effort was expended to determine analytically design constraints of pulsed mirror structures, to determine fabrication techniques of post mounted faceplate mirrors, and develop testing procedures for determining mirror surface distortion. A review of the results to date is presented in the following sections.

5.1 Analysis of Mirror Faceplate Distortion. (S) Analytical studies of the distortion of post-mounted faceplates under various forms of laser loading were performed. Laser pulses of varying spatial amplitude and a uniform pressure load on the faceplate were studied. Two separate models of the post-mounted faceplate were used and the numerical results cross-checked with each other. Results indicate that, for laser pulse intensities as high as 2 MW/cm^2 and 100 μsec duration, and for pressure loadings as high as 1.0 atmosphere, mirror faceplate distortion can be held to well within diffraction limited accuracy if the proper faceplate post geometry is chosen. From these studies we can conclude the following: (1) Localized dynamic displacements of the faceplate between the posts are not large, for operating wavelengths of 5 microns with post spacing of at least 1.0 cm and for a mirror thickness of at least 0.1 cm. (2) The oscillatory portion of the faceplate transient response can be predicted by modeling the post support structure as a continuous elastic foundation. The oscillatory response is confined to a narrow annulus at the edge of the mirror. For the faceplate-post geometry considered, the width of this annulus is typically one-tenth of the mirror diameter (0.55 cm compared with a total mirror diameter of 5.0 cm, for example).

(U) A computer program of the analytical model has been developed to calculate parametric dependence of the mirror distortions. Given a particular mirror geometry and loading conditions, the faceplate response to a pulsed

thermal load and to a uniform pressure load can be predicted. The codes are sufficiently efficient that they can be used in an iterative manner.

(U) The mirror model consists of a circular plate supported by uniformly spaced posts. The effect of the laser energy absorbed by the faceplate is to increase its temperature. The intensity of absorbed energy decreases exponentially with mirror depth. Thus the effect of the incident laser radiation is to produce a nonuniform faceplate temperature. The effect of this nonuniform temperature is a thermal force and moment given by:

$$N^T = E_T Q^T / (1 - \nu), \text{ in kg/cm}$$

$$M^T = E_T h Q^T / 2(1 - \nu) \text{ in kg-cm/cm}$$

and Q^T is defined by:

$$Q^T = 21_o (1 - R)\, t_p / \pi J \rho c_p, \text{ in cm}^2/\text{cm-C}^o$$

where

E = Young's modulus of the mirror material (kg/cm^2)
ν = Poisson's ratio
α_T = Coefficient of thermal expansion per C^o of the mirror material
I_o = Incident radiation (w/cm^2)
R = Reflectivity of the mirror at the laser wavelength
t_p = Laser pulse duration (sec)
ρ = Mass density of the mirror material ($gm\text{-}sec^2/cm^4$)
C_p = Specific heat of the mirror material ($cal/gm\text{-}C^o$)
J = 4.187 conversion factor (joules/cal)

(U) Two models are used for analyzing the mirror response. In the first model, the mirror faceplate is supported by concentric rings. The uniform rings approximate rings of equally spaced posts. In the second model the mirror plate is assumed to be supported by a continuous elastic foundation. These two models predict essentially the same behavior, except that annular end effects are more pronounced in the model which assumes the elastic foundation.

(U) The problems studied can be divided into two groups:

(1) Transient response of the faceplate during the loading, and

(2) The response or steady state faceplate distortion with no heat dissipation.

(S) The transient response is analyzed using the continuous model. The classical spectral expansion is used to represent the transient behavior requiring a complete knowledge of the free vibration characteristics (frequencies and corresponding mode shapes) of the mirror plate. A computer program has been developed for calculating the free vibration frequencies, the corresponding mode shapes, the steady state solution, and the transient response of the mirror during the laser pulse. The mirror model used has been parametrized typically as follows:

a = radius of mirror plate = 5 cm

h = thickness of mirror plate = 0.2 cm

ℓ_p = height of the posts = 1 cm

d_p = diameter of the posts = 0.1 cm

b = spacing between posts = 0.5 cm

The laser load is assumed to be:

I_o = incident laser intensity = 2 MW/cm^2

t_p = laser pulse duration = 100 μsec

R = reflectivity of the mirror at the laser wavelength = 98.0%

(U) In Figure 23 the displacement of the mirror faceplate is plotted as a function of time. In Figure 24 the steady state displacement at the end of the laser pulse is plotted together with the transient response. Two conclusions are drawn from Figures 23 and 24: (1) The distortions of the mirror faceplate, for the design chosen, are acceptable (small compared to a laser wavelength). Also note that the transient response shows the same general features of the steady state response. (2) The worst distortion of the faceplate is confined to an annular region at the mirror edge. The width of this annulus is approximately given by

$$w_a = \left[\frac{4}{3\pi(1-\nu^2)} \left(\frac{b}{d_p} \right)^2 \cdot h^3 \ell_p \right]^{1/4}$$

The distortion in the central 70% area of the plate is well within the acceptable level of 10^{-5} cm or $\lambda/50$ for the case considered at the laser wavelength of 5 microns.

(U) The annular width calculated is comparable to the post spacing, indicating that although gross qualitative features are the same, significant local (intrapost) differences can result between finite post-supported versus continuously-supported mirror faceplates.

(U) Figure 25 shows a post mounted mirror model. The diameter of the central post (dp_1) is assumed variable. All other posts have a constant diameter (d_p = 0.1 cm). The post spacing is kept constant (b = 0.5 cm). The mirror faceplate is divided into segments between posts. The solution for each plate segment is obtained in closed form using thin plate theory and by requiring continuity and equilibrium at the post joints. The final solution for the entire faceplate is then obtained. The following three cases considered are shown in Figure 25.

(1) A uniform temperature rise over the faceplate with $m_T(r) = M_T =$ constant, where m_T and M_T are thermal moments.

(2) A generalized Gaussian temperature distribution over the faceplate $m_T(r) = M_T \exp(-nr^2/a^2)$, with n = 1, 2, 3.

(3) A uniform pressure load of p = 14.7 psi.

(S) The results of the analysis for these cases are shown in Figures 26, 27, 28 and 29. In Figure 26, the distortion due to a constant temperature distribution resulting from an intensity $I_o = 1.2$ Mw/cm^2 is shown. It is apparent that the mirror faceplate distortion has generally a wavy form with the amplitude diminishing towards the center. In Figure 27, the distortions due to the generalized Gaussian loads are shown. The same wavy form is still apparent. The nonuniform thermal moments tend to distort the central portion of the mirror also, but not as severely as the annulus.

(U) In Figures 28 and 29, the distortions shown consider the case of a static pressure of one atmosphere across the faceplate for two faceplate thicknesses and two diameters of 0.1 cm and 0.06 cm, respectively, for the central post. Note that the thinner central post significantly reduces the distortion in the center. All other design values are identical. This result is typical of the type of design detail that can be investigated using the analytical techniques discussed.

5.2 Mirror Faceplate Fabrication. (U) The investigation of fabrication techniques for post-mounted mirror faceplates consisted of three parts: (1) material selection, (2) development of polishing techniques, and (3) development of methods for fabricating the multipost faceplate structure.

(S) Of the various candidate mirror materials, a beryllium copper alloy was selected as providing the best combination of desirable thermal and mechanical characteristics. The specific alloy chosen was Berylco 10, a high strength material with high thermal conductivity, high oxidation resistance, and good machining characteristics. Heat treatment to release fabrication stresses and also solution treating and brazing are all easily accomplished with this alloy. When coated for 99.0% reflectivity, these mirrors should withstand 100 μs laser pulses at 2 MW/cm^2.

(U) Polishing techniques were also developed for materials such as Berylco 10, Berylco 25, molybdenum, copper, quartz, pyrex, and germanium. The preferred mirror material, Berylco 10, has been polished to $\lambda/20$ flatness and with acceptable scratch/dig ratios. Berylco 25 hole-coupling mirrors have been polished to diffraction limited flatness and are being used in the E-beam pulsed laser experiments.

(U) Fabrication of the faceplate-post structure was explored using machining, brazing, and welding. Machining the faceplate and posts from a single piece of material was successfully accomplished on a small mirror and should yield the most thermally stable structure, but obtaining satisfactory cutters at reasonable cost has been a problem. Brazing is the least expensive method of joining posts to the faceplate but residual stresses set up between the braze and mirror material may later cause faceplate distortion. Welding the posts to the faceplate has been attempted using capacitor discharge welders, spot welders, and a Q-switched ruby laser. Weld quality has not been satisfactory although a refinement of either the capacitor discharge welder or laser welder might well yield acceptable joints. Any of the above techniques should be adequate. If a multipost faceplate is required for the near term, machining the faceplate-post structure from a single piece of material will be used for this program.

5.3 Optical Test Facility. (U) A general purpose laser interferometer and holography facility for testing and evaluating mirrors, windows, and laser media is under development. Figure 30 is a diagram of one of several interferometers that can be set up using the same set of optics. Shown is a standard Mach-Zehnder interferometer with pulsed ruby or continuous wave He-Ne laser illumination. The interferometer portion consists of two beam splitters and two mirrors and has a minimum clear aperture diameter of 10 cm. For testing laser mirrors statically or under transient loading, the test mirror will replace either one of the two interferometer mirrors. For testing windows, the test piece can be inserted in one of the beam paths. (The setup can also be readily converted to the Twyman-Green configuration, a conventional interferometer for testing mirrors and windows.) Optical components for this setup are being purchased or fabricated, and the setup is expected to be completed shortly.

(U) Three types of illumination can be used with the interferometer. For static evaluation of mirrors or windows a one milliwatt helium-neon laser will be used. For testing mirrors under pulsed loading, a pulsed ruby laser constructed at Northrop will be used. Finally, for applications requiring high level continuous illumination, a 100 milliwatt Coherent Radiation Model 54 Argon laser will be used.

(S) A xenon flash lamp loading setup for simulation of pulsed thermal loads on laser mirrors is also under development. The design is for a peak intensity of 40 kilowatts per cm^2 over an area of ~20 cm^2 and a pulse duration of ~100 μsec. To test a sample mirror, its substrate surface will be finished so that ~50% of this input power will be absorbed. This will simulate a loading of 2 MW/cm^2 on an operational mirror that absorbs less than 1% of the incident power. Figure 31 is a block diagram of the flash lamp loading setup consisting of an energy storage capacitor bank, a high

voltage charging power supply, a flash lamp trigger power supply and the flash lamp bank itself. The latter consists of four linear xenon lamps and a diffuse cavity reflector. The setup will be tested shortly.

6.0 REFERENCES (U)

1. M. L. Bhaumik, W. B. Lacina, and M. M. Mann, IEEE J. Quant. Elect. QE-8, 150 (1972); presented at Conf. on Laser Eng. Appl. Washington, D. C. (June 1971).

2. W. B. Lacina, "Kinetic Model and Theoretical Calculations for Steady State Analysis of Electrically Excited CO Laser Amplifier System, Final Report: Part II," NCL Report 71-32R, (August 1971).

3. W. B. Lacina, "Steady State Kinetics of an Electrically Excited CO Laser Amplifier," (January 1972) submitted for publication.

4. W. B. Lacina and M. M. Mann, "Transient Oscillator Analysis of a High Pressure Electrically Excited CO Laser," (April 1972) submitted for publication.

5. W. L. Nighan, Phys. Rev. 2A, 1989 (1970).

6. J. D. Daugherty, E. R. Pugh, and D. H. Douglas-Hamilton, presented at 24th Annual Gaseous Elect. Conf., Gainesville, Florida (October 1971).

7. C. A. Fenstermacher, M. J. Nutter, W. T. Leland, and K. Boyer, Appl. Phys. Lett. 20, 56 (1972); presented paper at 24th Annual Gaseous Elect. Conf., Gainesville, Florida (October 1971).

8. B. B. O'Brien, "Plasma Characteristics of an Electron Beam Excited High Pressure Discharge," NLSD Report 72-8R (March 1972).

9. A. G. Fox and T. Li, "Resonant Modes in a Maser Interferometer," Bell Sys. Tech. J., Vol. 40, pp 453-488, (March 1961).

10. R. A. McClatchey, "Atmospheric Attenuation of CO Laser Radiation," AFCRL 71-0370, Environmental Research Papers, No. 359 (July 1971).

11. M. L. Bhaumik, "CO Laser Line Selection Technique," Northrop Corporation Laser Systems Department Report NLSD 71-7R, (December 1971).

12. M. L. Bhaumik, "CO Laser Line Selection for High Atmospheric Transmission," Applied Physics Letters, to be published 1 May 1972.

(U) TABLE I. OSCILLATOR PARAMETRIC CALCULATIONS. (U)

Label	p(CO) (torr)	$p(N_2)$ (torr)	T (%)	γ (%/pass)	T_{pulse} (μsec)	T_{laser} (μsec)	T_{mol} (°K)	T_{rot} (°K)	W (kW/cm^3)	Optical Output Efficiency	Energy (J/cm^3)
FH87X72	250	300	20	0	0-140	< 10	100	125	16.6-12.0	68.3	1.20
FH940DD	100	650	10	0	0-100	< 10	125	125	23.4-16.4	74%	1.06 + 0.23
FH6604Y	100	650	10	0	100-150		125	125	0		
FH950DE	100	650	10	0	0-100	< 10	125	125	23.4-15.1	52%	0.66 + 0.19
FH67045	100	650	10	0	100-150		125	125	0		
FH430SW	100	650	10	0	0-150	< 10	125	125	23.4-16.0	56.4	1.42
FH18010	250	500	2	10	0-300	210	270	350	1.7-0.9	1.5	0.0059
FH4300H	250	500	2	10	300-600		270	350	0.0		
FH5505U	250	500	4	7	0-300	200	270	350	1.7-0.9	1.1	0.018
FH85081	250	500	20	0	0-300	70	150	200	5.5-3.5	13.7	
FH180K5	250	500	20	0	0-300	110	150	200	2.7-2.0	30.7	0.20
FH690Y1	250	500	20	0	0-300	10	150	200	13.5-9.8	68.3	2.06
FH72020	250	500	10	0	0-300	100	150	200	2.7-2.0	32.6	0.21
FH7302E	250	500	20	0	0-300	50	150	200	9.0-5.6	59.0	1.06
FH70014	250	500	20	0	0-300	270	300	400	1.3-0.8	0.3	0.001
FH7602P	250	500	5	0	0-300	110	300	400	3.7-2.0	29.1	0.21
FH80028	250	500	5	0	0-300	150	300	400	2.5-1.5	15.7	0.08
FH190MU	250	500	5	5	0-300	230	300	400	1.6-1.0		
FH610DF	250	500	5	5	0-300	200	300	400	1.9-1.1	5.6	0.023
FH11ABX	250	500	5	0	0-300	180	300	400	1.9-1.0	7.0	0.029

UNCLASSIFIED

(U) TABLE II. e-FOLDING DISTANCES FOR CO LASER LINES THROUGH A 1 km HORIZONTAL ATMOSPHERIC PATH AT SEA LEVEL. (U)

Vibrational Band	Rotational Line	ν (cm^{-1})	$1/k_{mw}$ (km)
6 → 5	P10	1973.285	14.49
	P 9	1977.264	13.51
5 → 4	P16	1974.362	15.15
	P15	1978.575	23.26
	P14	1982.754	12.99
	P 9	2003.154	18.52
4 → 3	P15	2004.326	22.73
	P13	2012.723	11.90
	P10	2025.068	13.70
	P 9	2029.117	35.71
	P 8	2033.132	43.48
	P 7	2037.113	13.70
3 → 2	P16	2025.866	58.82
	P15	2030.148	21.28
	P13	2038.615	19.61
	P10	2051.066	10.64
	P 9	2055.150	55.56
	P 8	2059.200	11.49
2 → 1	P19	2038.573	20.00
	P17	2047.371	22.73
	P16	2051.721	10.64
	P15	2056.039	66.67
	P12	2068.795	38.46
	P11	2072.980	17.24
	P10	2077.133	41.49
	P 9	2081.251	52.63
	P 8	2085.337	47.62
1 → 0	P18	2068.841	38.46
	P17	2073.259	14.71
	P16	2077.645	35.71
	P14	2086.318	35.71
	P12	2094.859	28.57
	P11	2099.080	76.92
	P10	2103.267	31.25
	P 8	2111.541	43.48
	P 7	2115.627	13.33
	P 6	2119.680	166.67

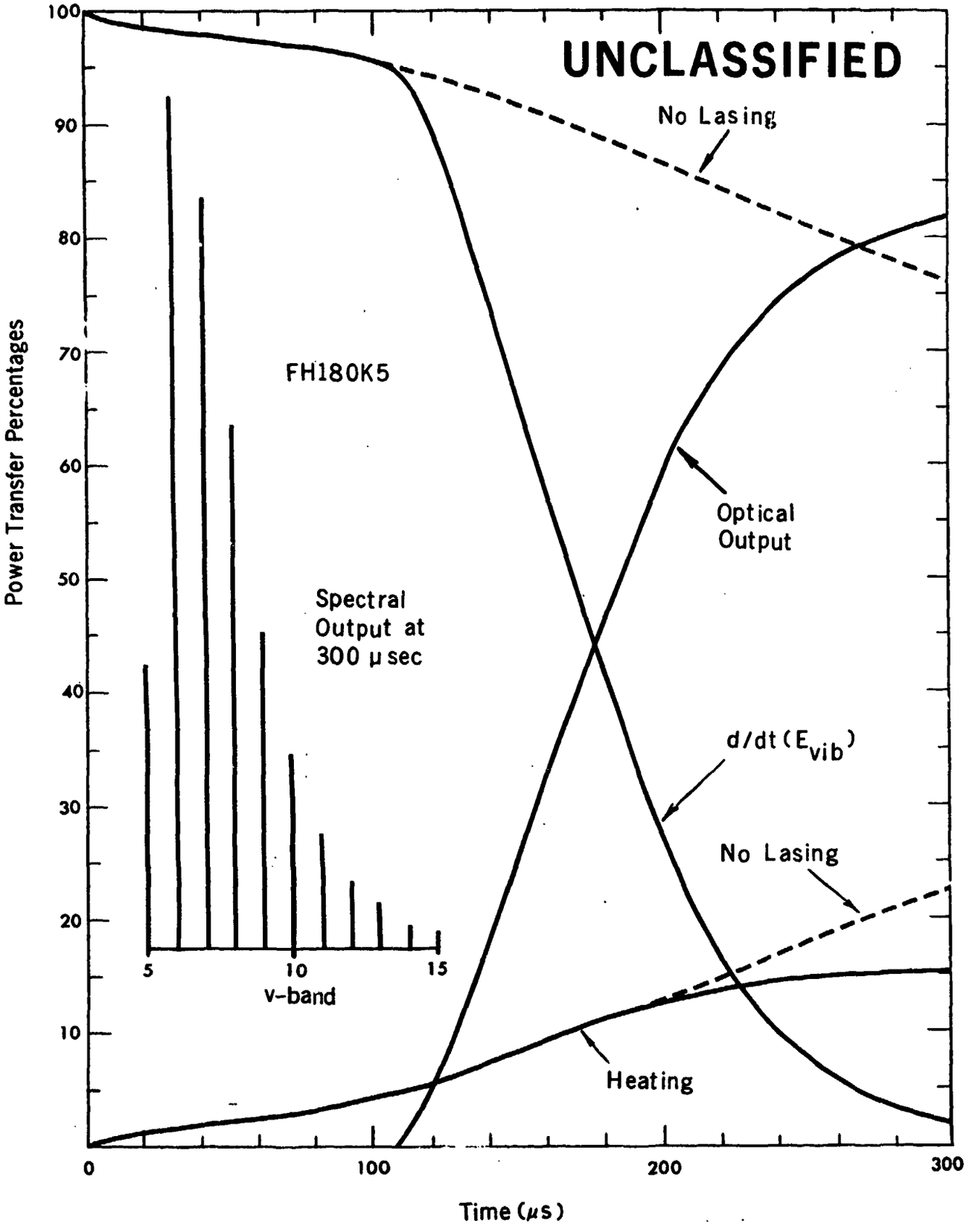

(U) Figure 1. Percentage power transfer in a pulsed oscillator (Case FH180K5). (Parameters are summarized in Table I). (U)

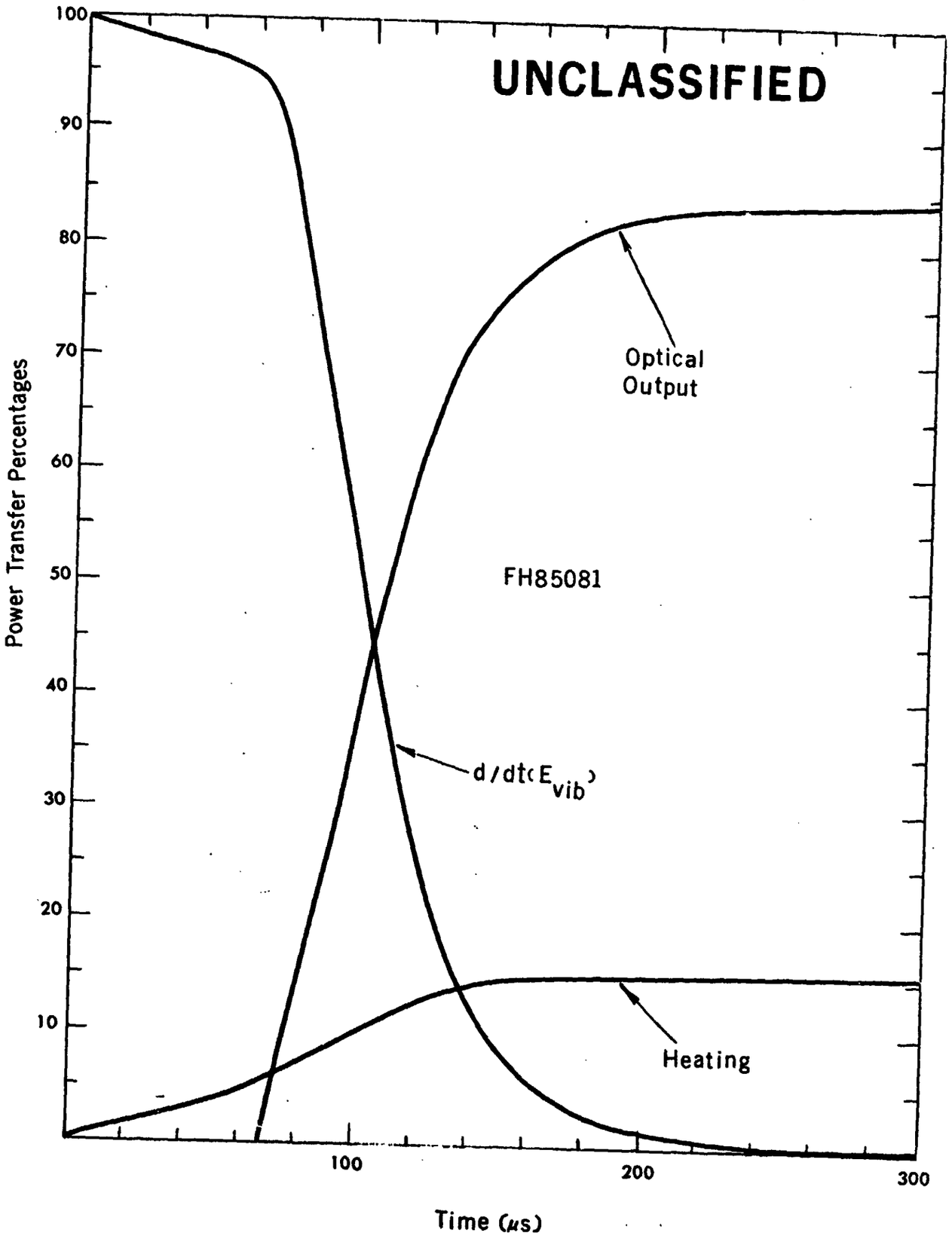

(U) Figure 2. Percentage power transfer in a pulsed operation (Case FH85081). (Parameters are summarized in Table I). (U)

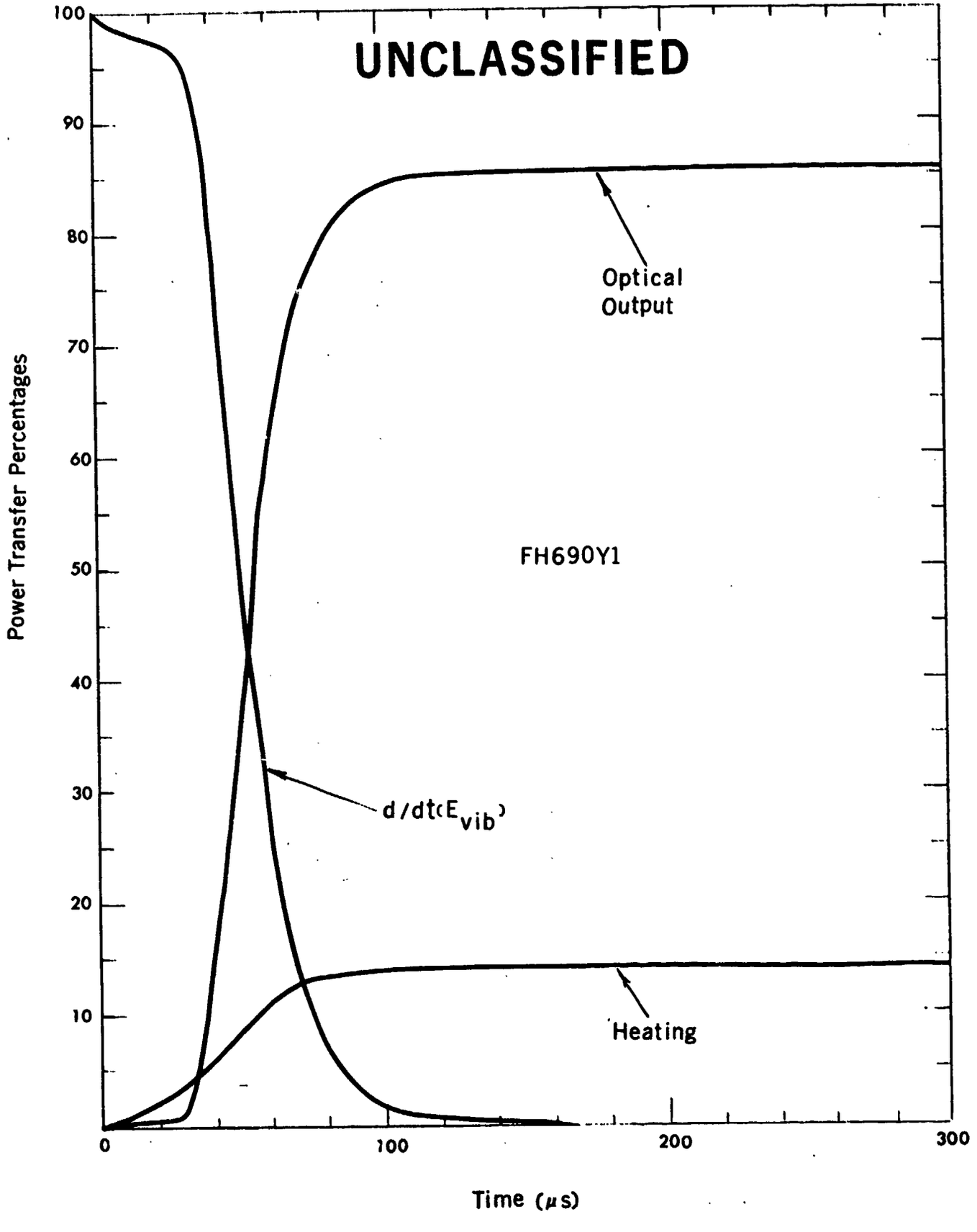

(U) Figure 3. Percentage power transfer in a pulsed oscillator. (Case FH690Y1) (Parameters are summarized in Table I). (U)

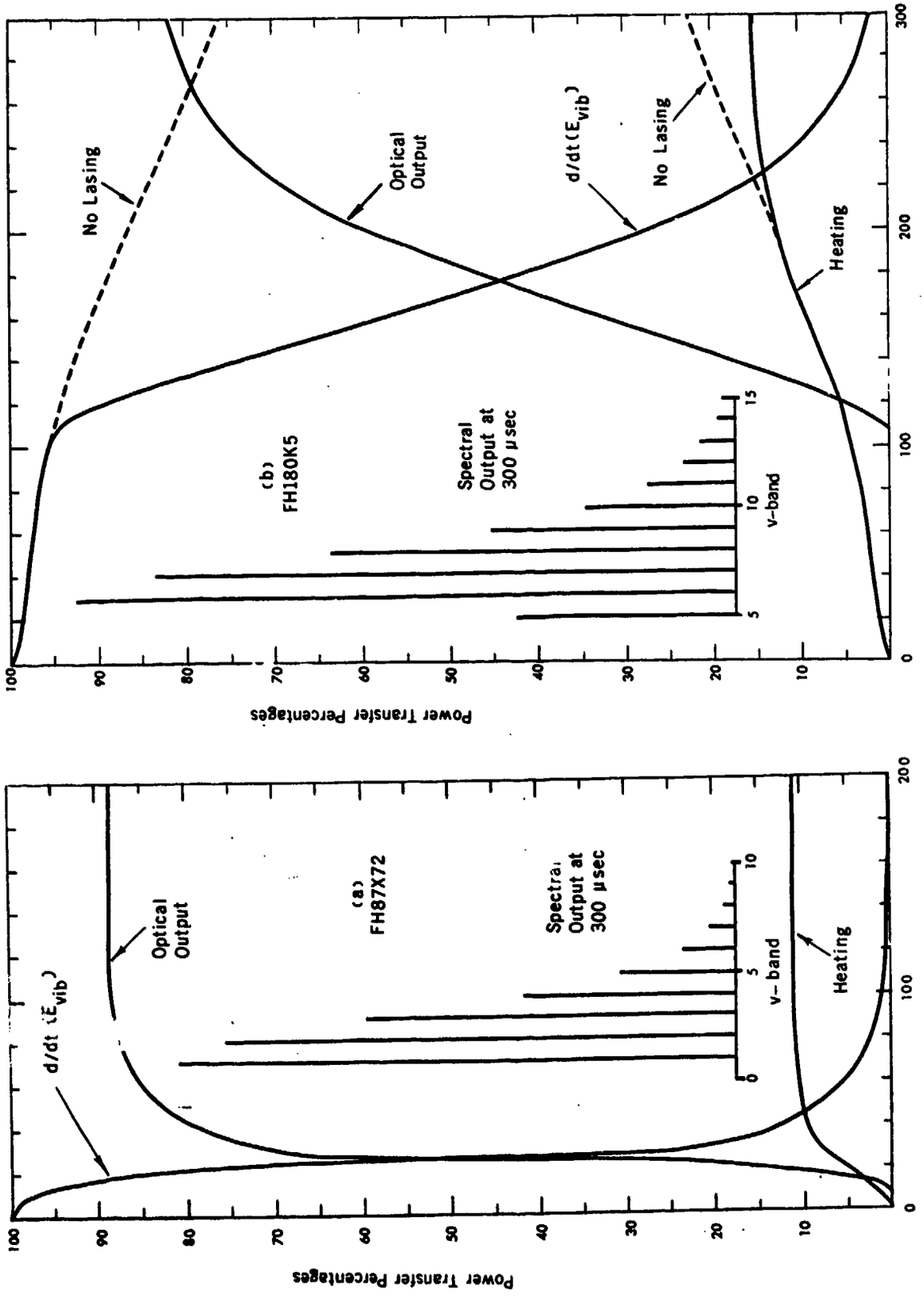

(U) Figure 4. Percentage power transfer in a pulsed oscillator. (Case (a) FH87X72, Case (b) FH80K5). (Parameters are summarized in Table I.) (U)

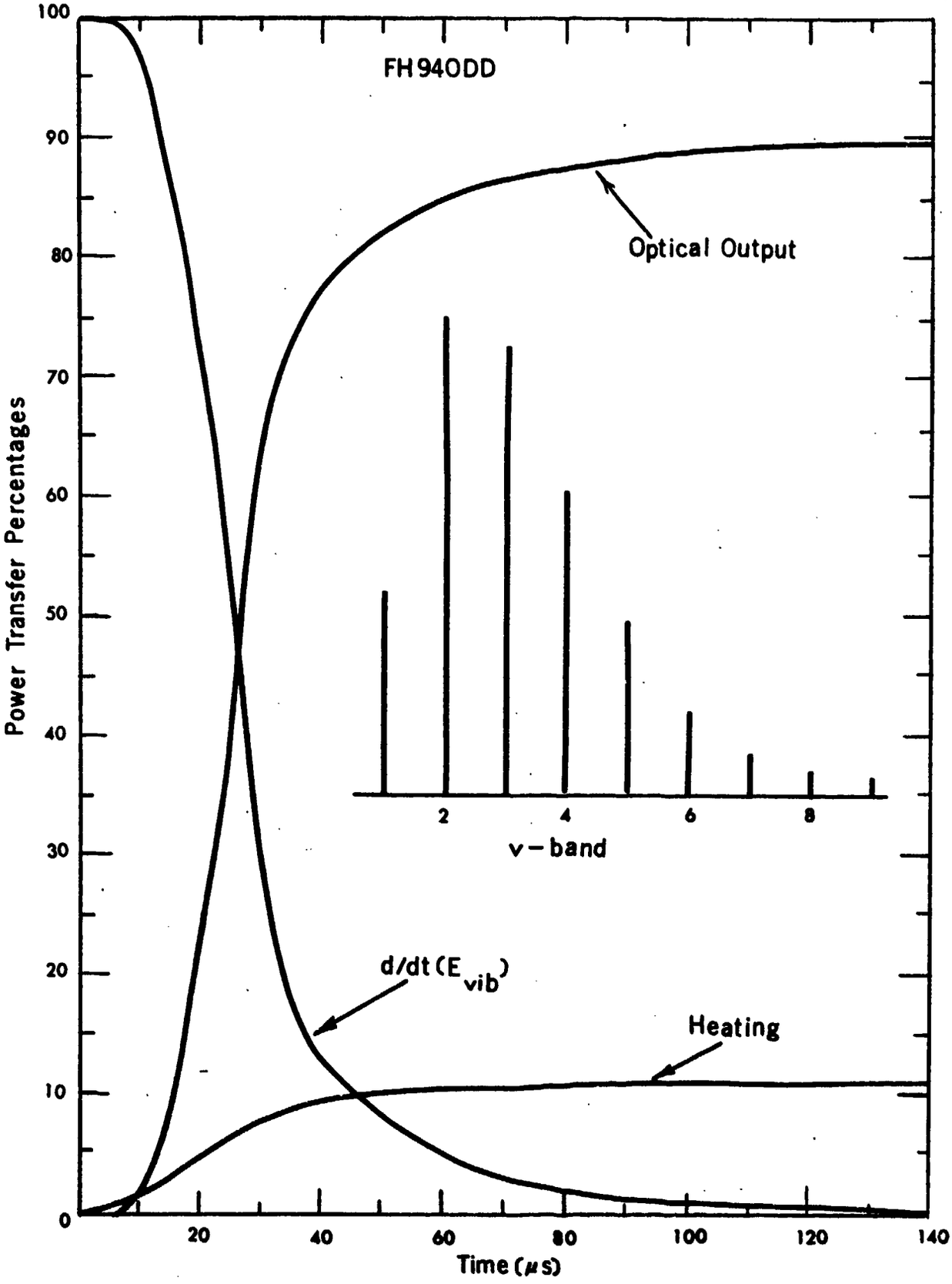

(U) Figure 5. Percentage of power transfer in a pulsed operation without line selection - Case FH940DD). (Parameters are summarized in Table I.) (U)

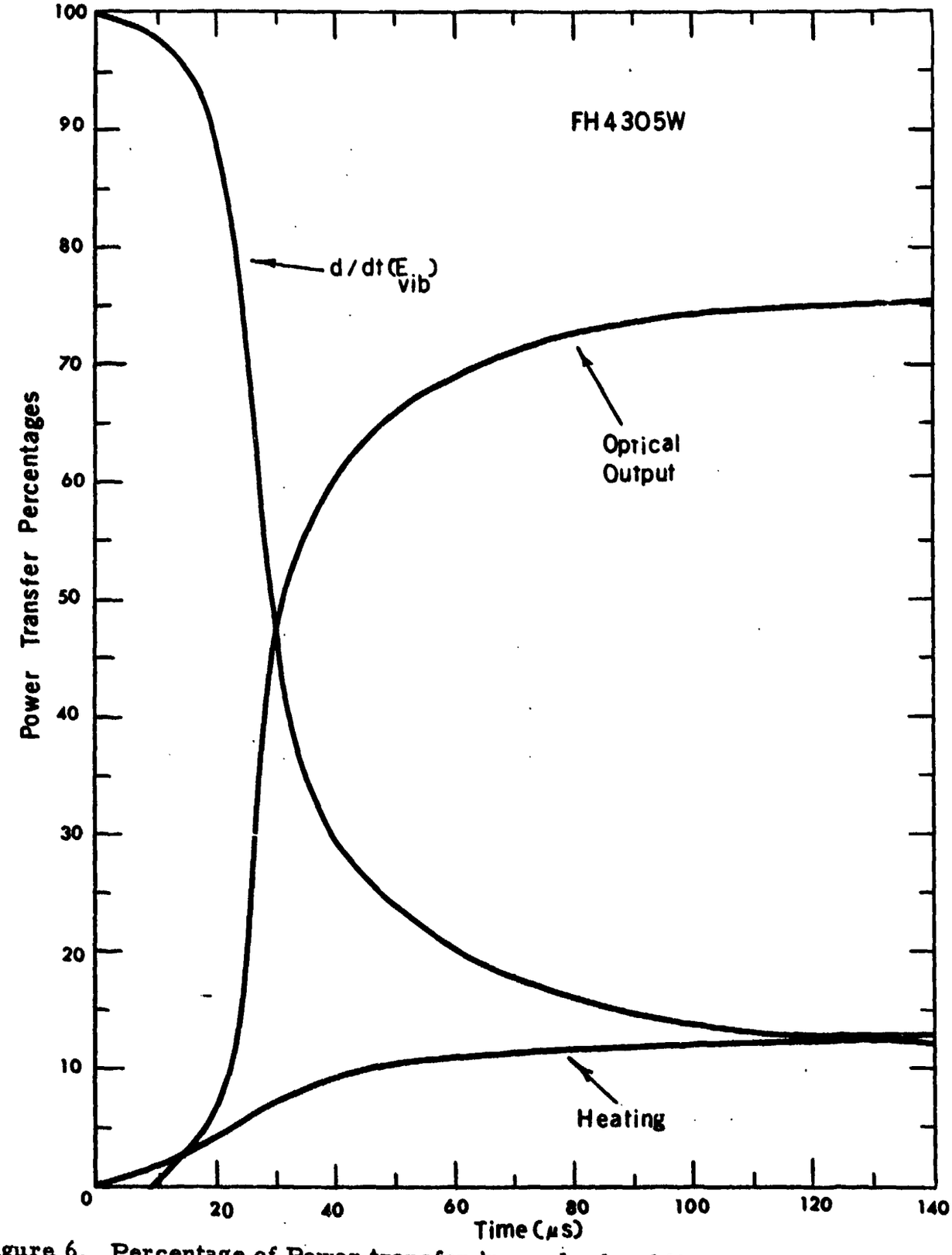

(U) Figure 6. Percentage of Power transfer in a pulsed and line selected operation (Case FH4305W). (Parameters are summarized in Table I.) (U)

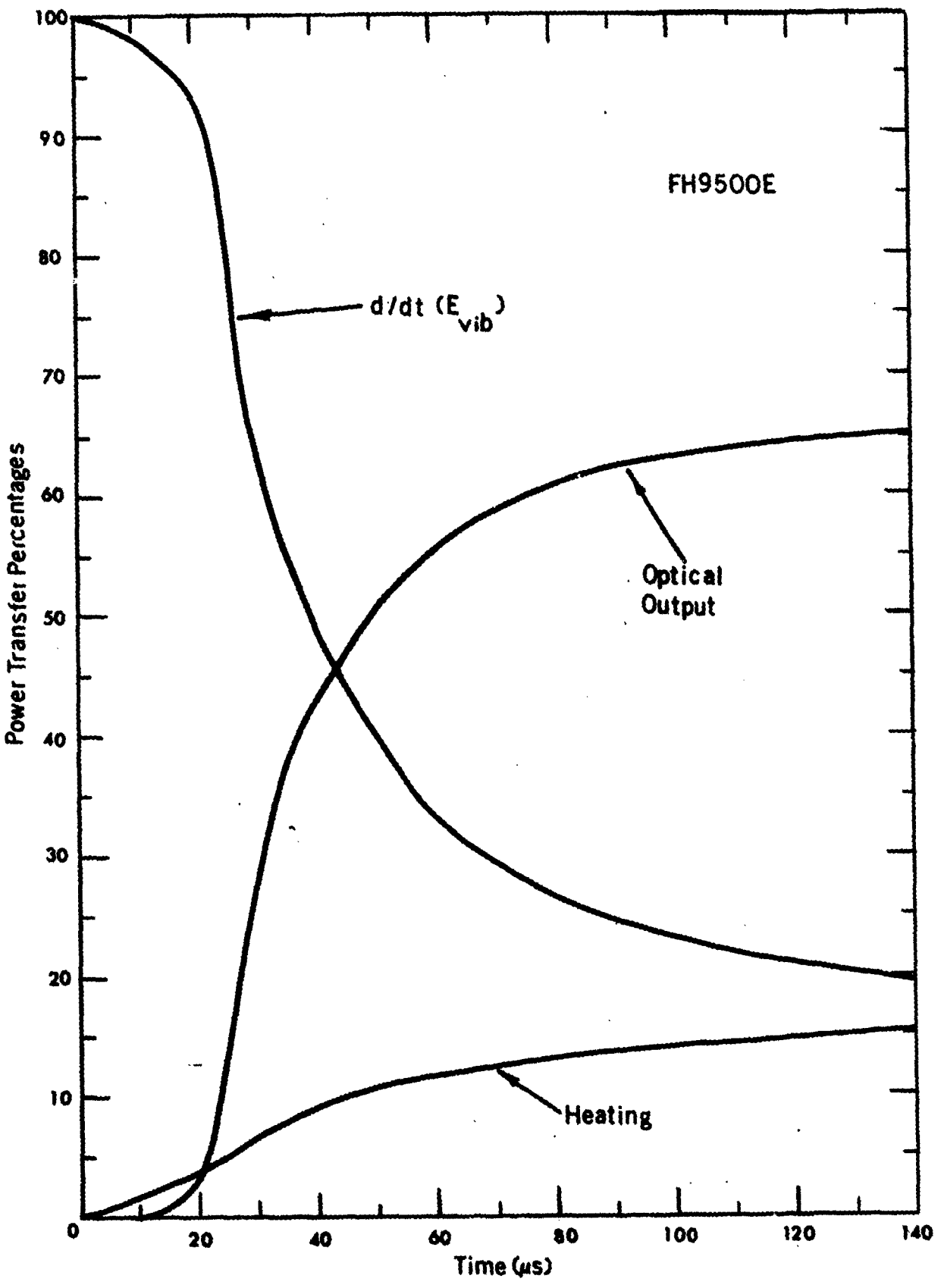

(U) Figure 7. Percentage of power transfer in a pulsed and line selected operation (Case FH9500E). (Parameters are summarized in Table I.) (U)

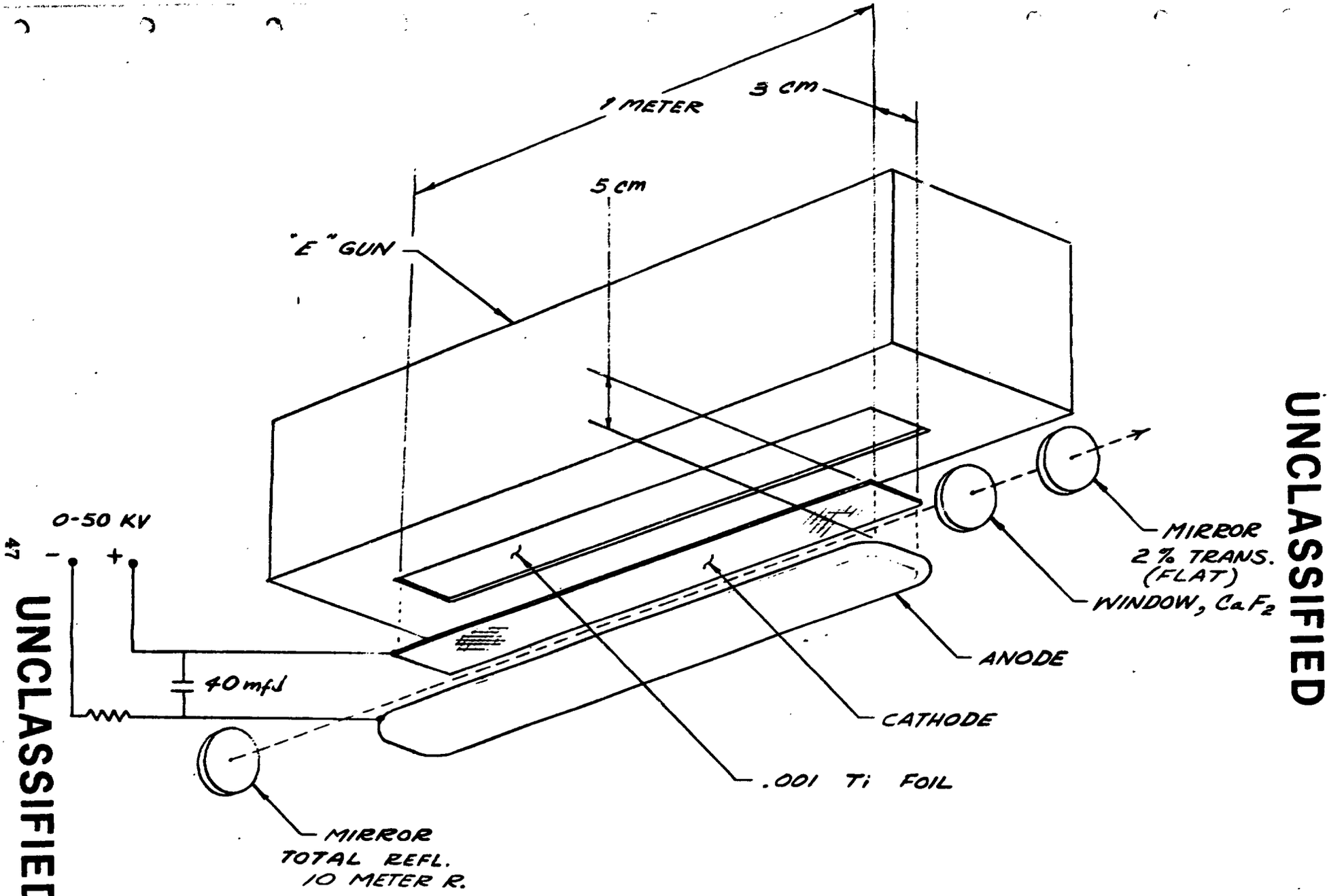

UNCLASSIFIED

(U) Figure 8. Schematic diagram of the E-beam device. (Room temperature experimental parameters shown.) (U)

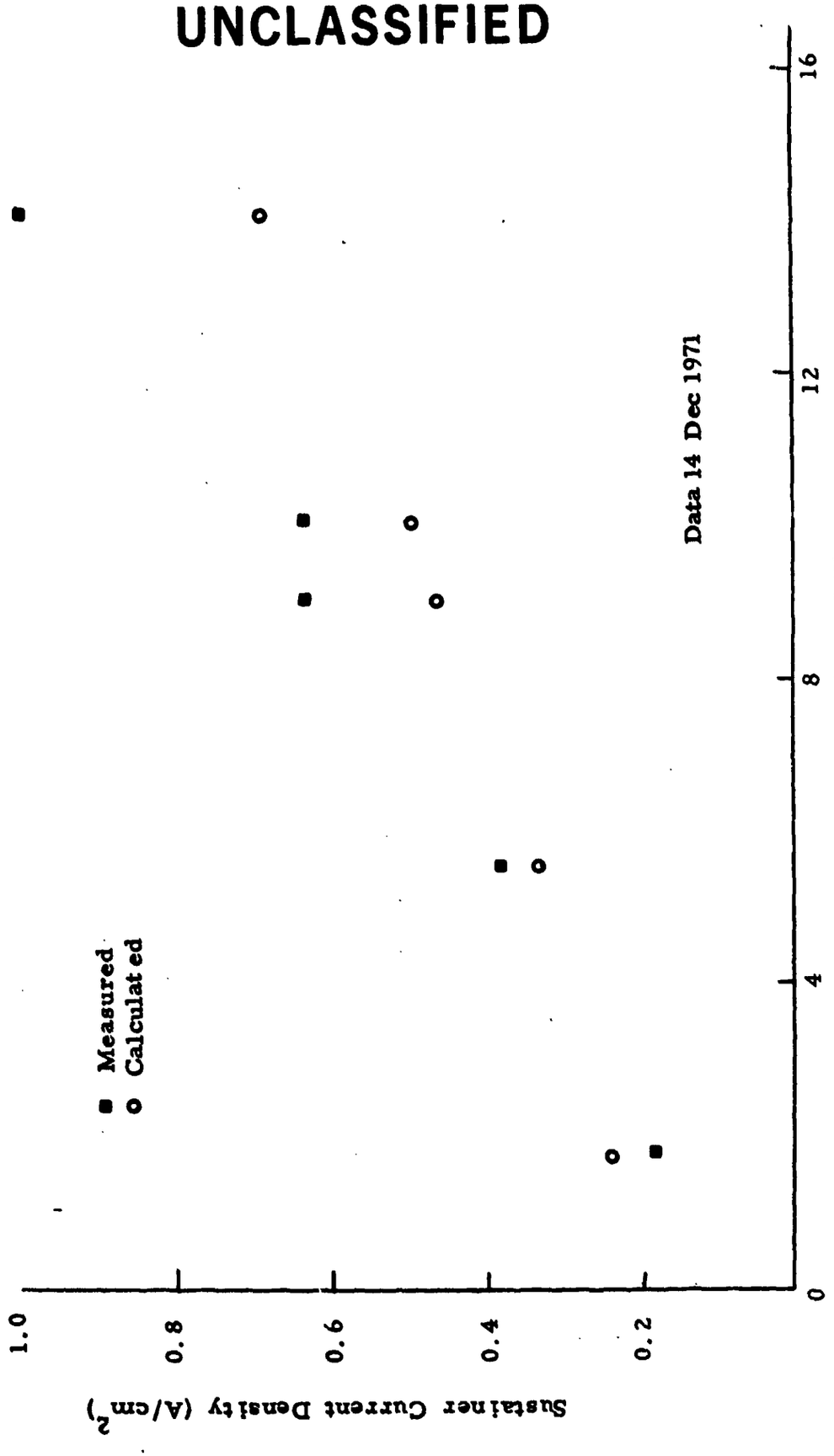

(U) Figure 9. Sustainer current density versus sustainer voltage. (U)

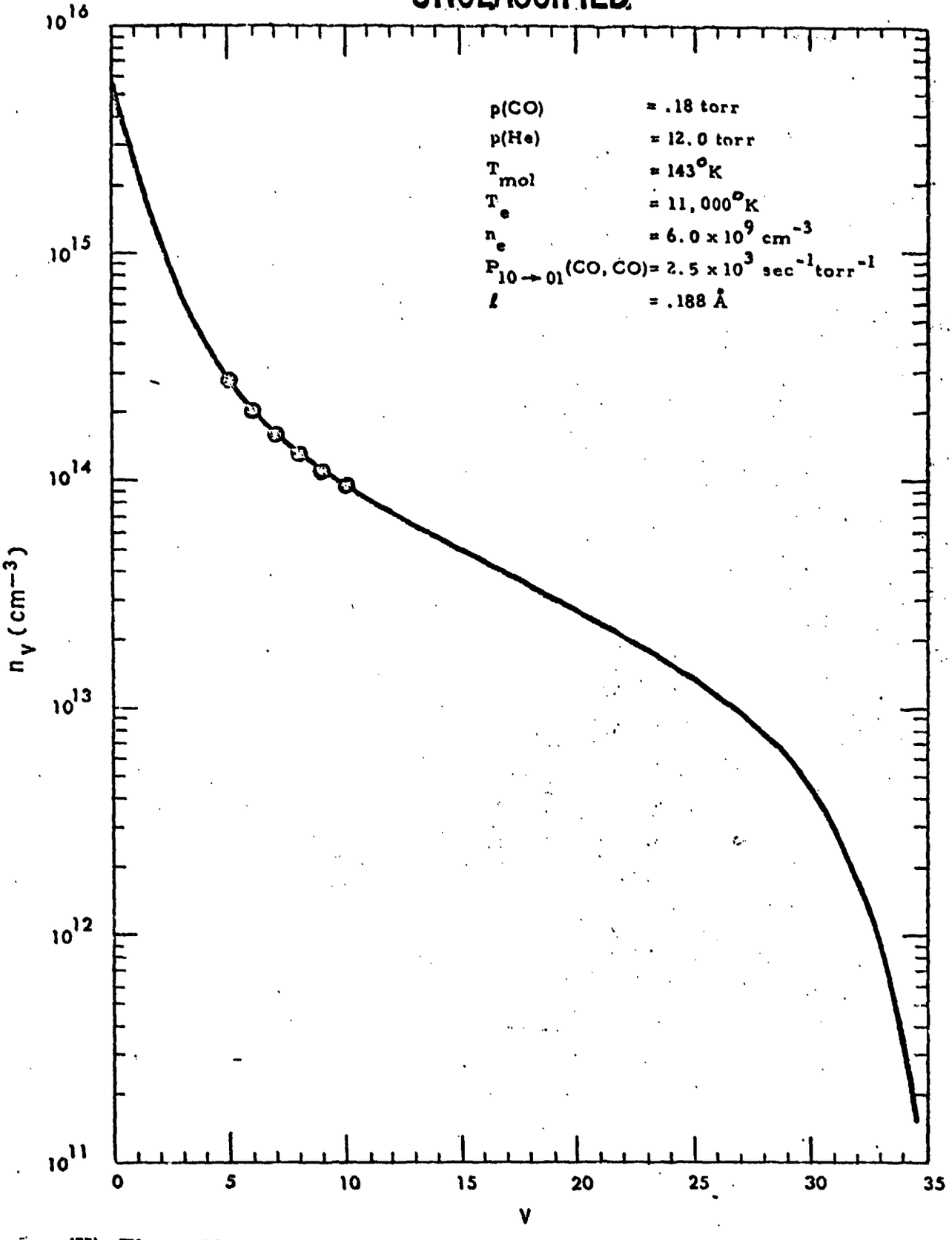

(U) Figure 10. Population densities for a cw CO amplifier. (U)

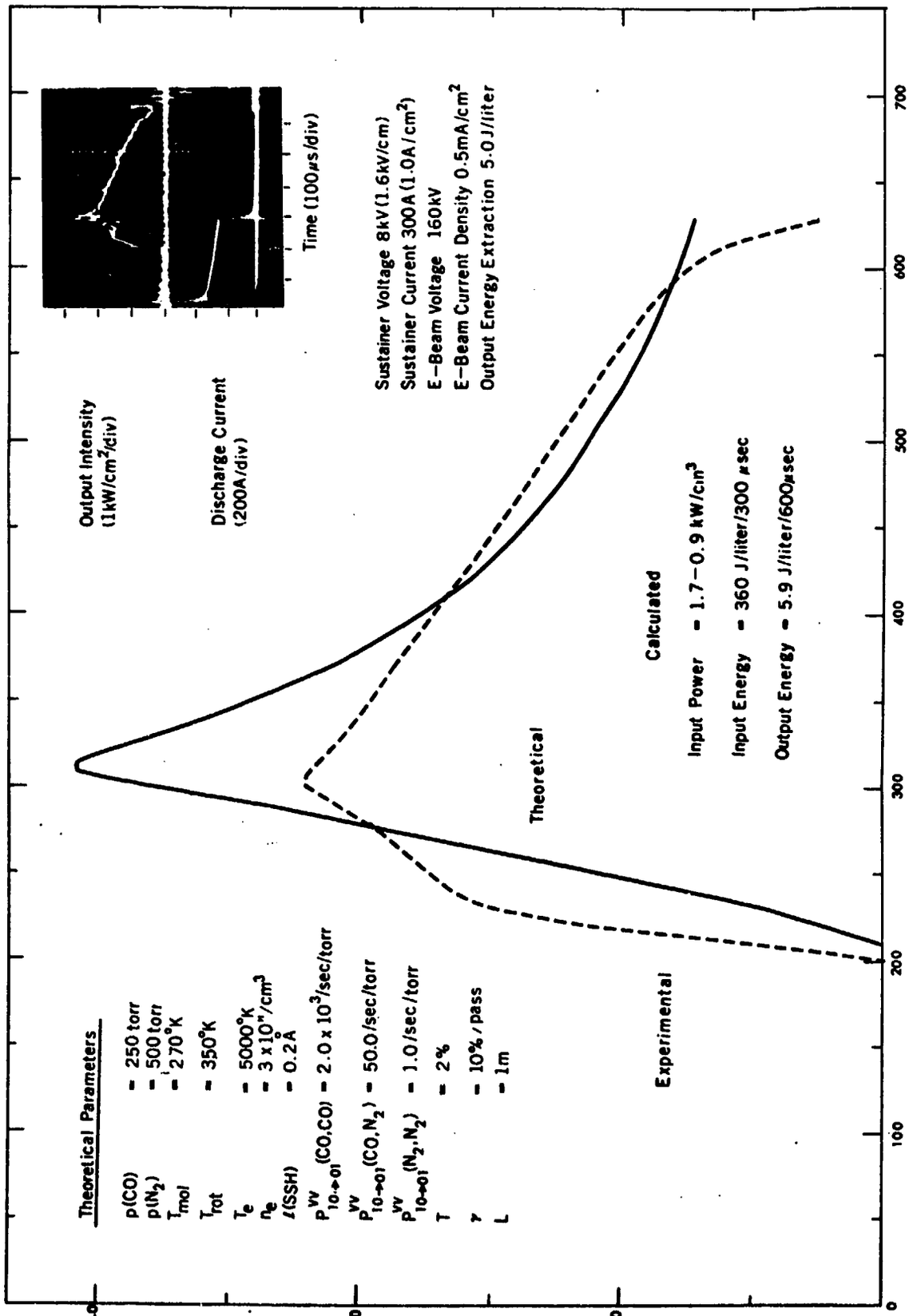

(U) Figure 11. Experimental data and theoretical predictions for the CO E-beam. (U)

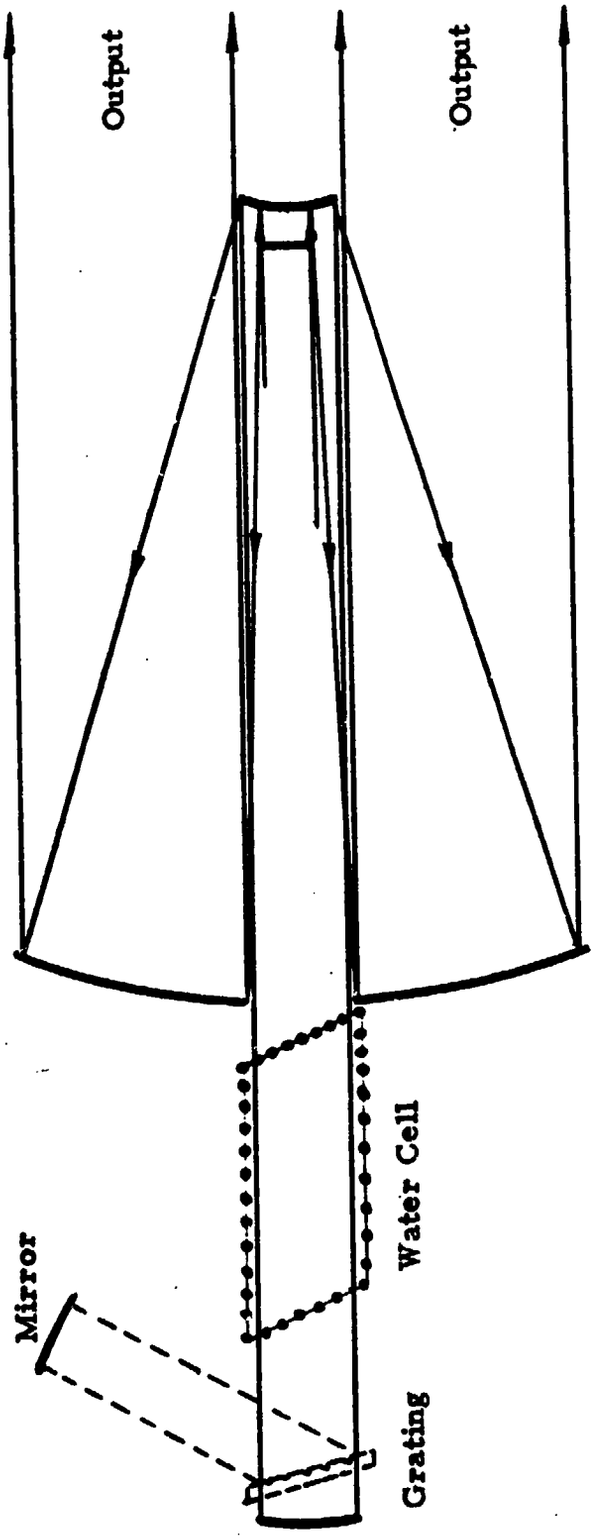

(U) Figure 12. Resonator configuration including possible line selection components. (U)

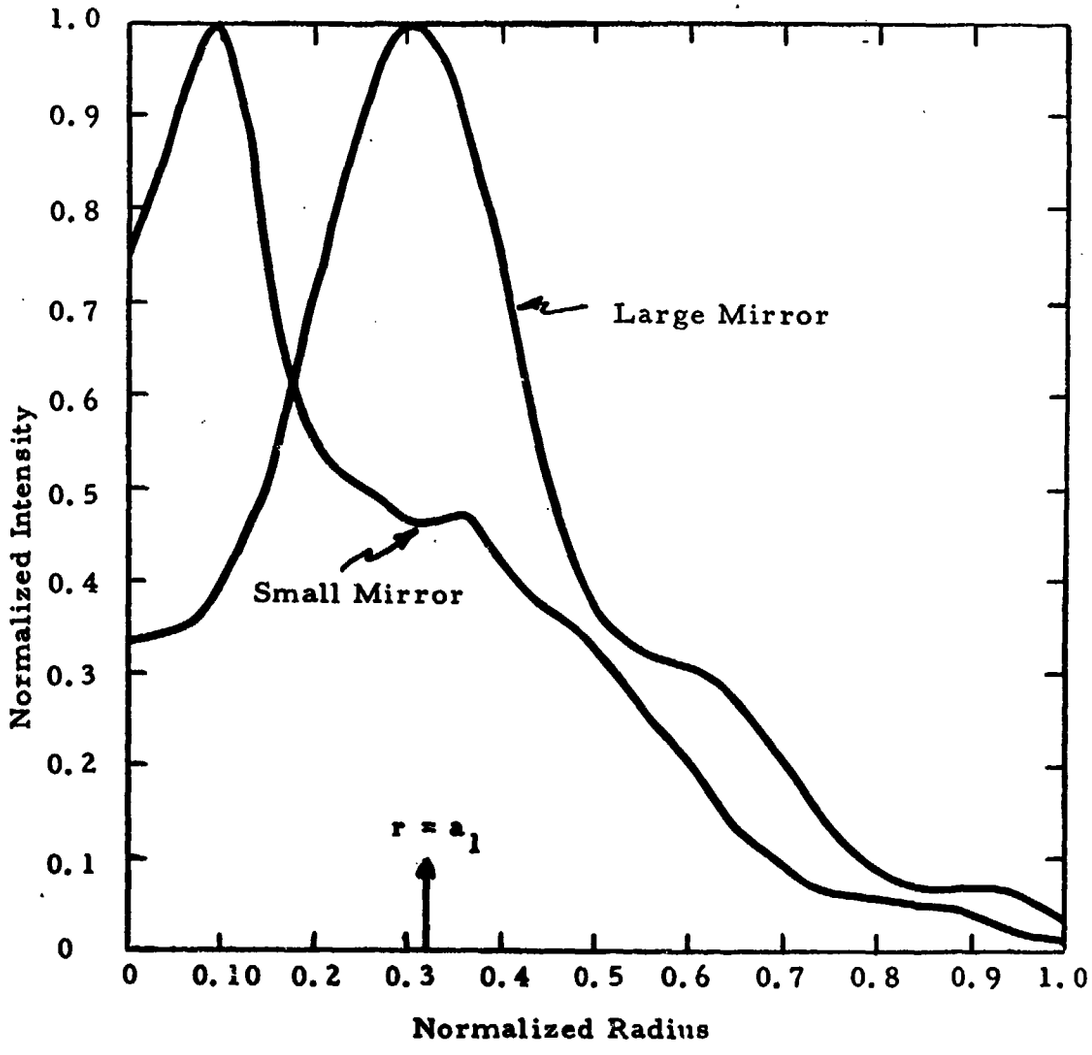

$M = 3.0$
$FN = 6.0$
$FN_{eff} = 2.0$
$\delta = 0.717$

(U) Figure 13. Intensity profiles on mirrors for confocal, unstable resonator. (U)

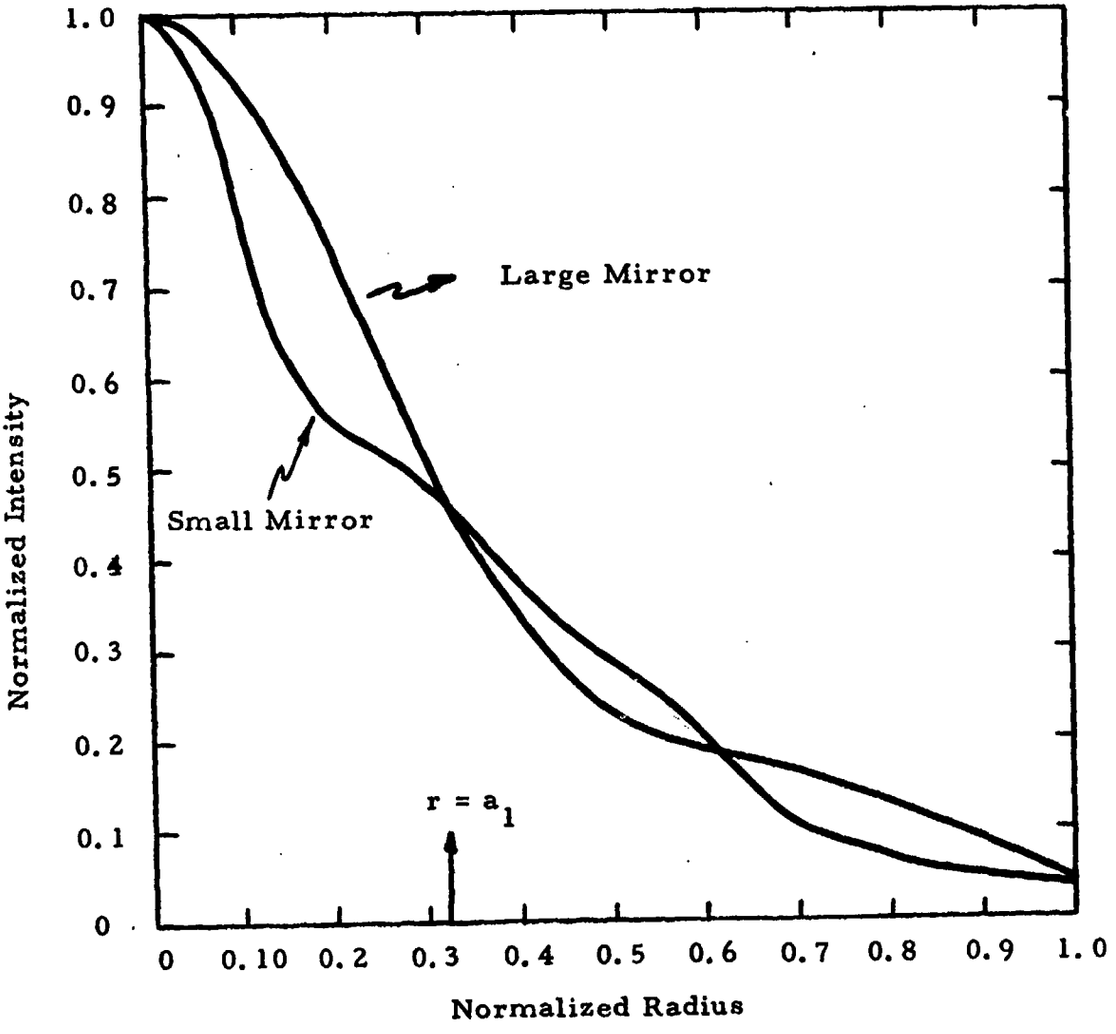

$M = 3.0$
$FN = 3.0$
$FN_{eff} = 1.0$
$\delta = 0.750$

(U) Figure 14. Intensity profiles on mirrors for confocal, unstable resonator. (U)

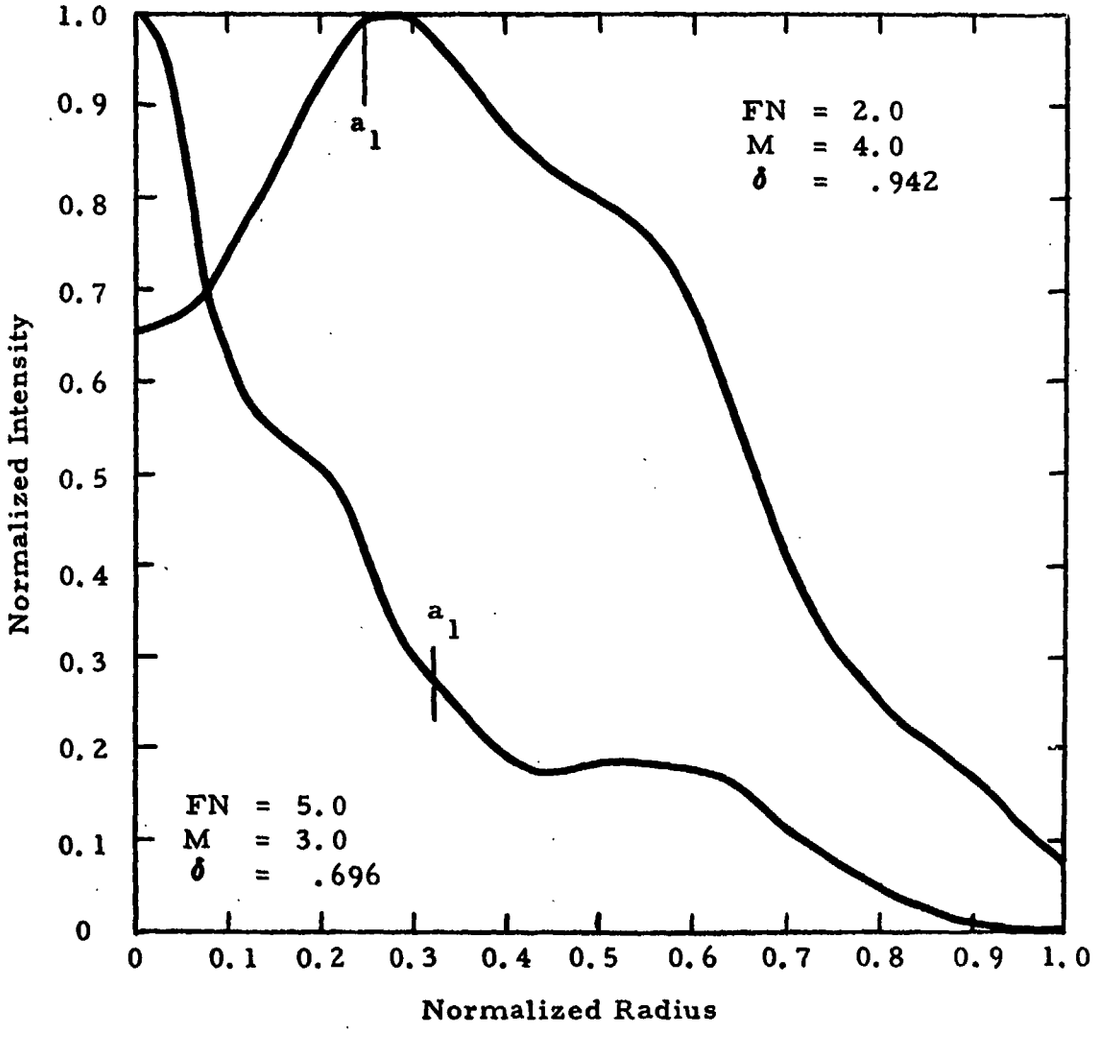

(U) Figure 15. Intensity profiles at the output mirror for two confocal, unstable resonators. (U)

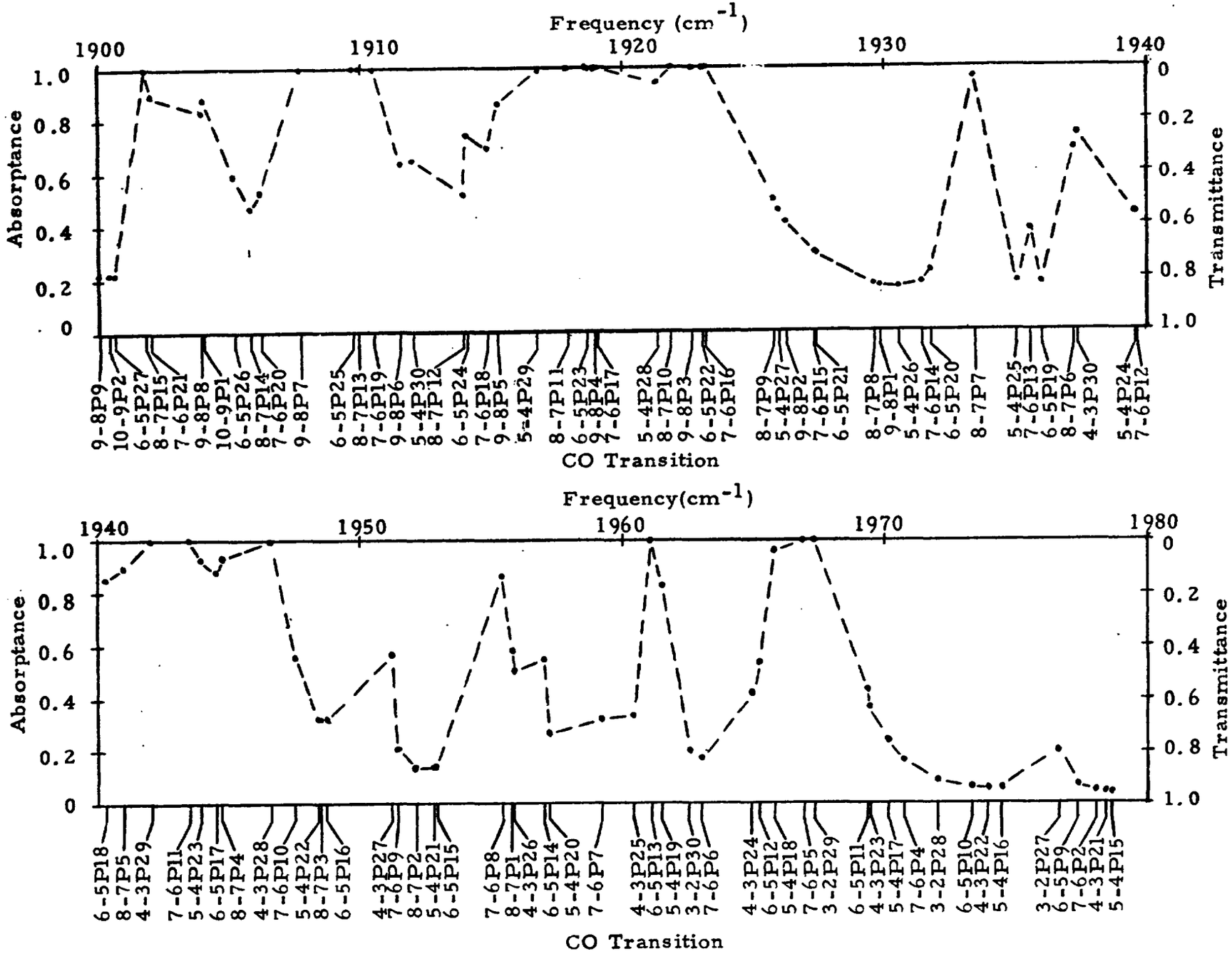

(U) Figure 16a. Absorptance-Transmittance of CO laser frequencies for a 1-Km horizontal atmospheric path at sea level (water vapor and nitrogen only). (U)

UNCLASSIFIED

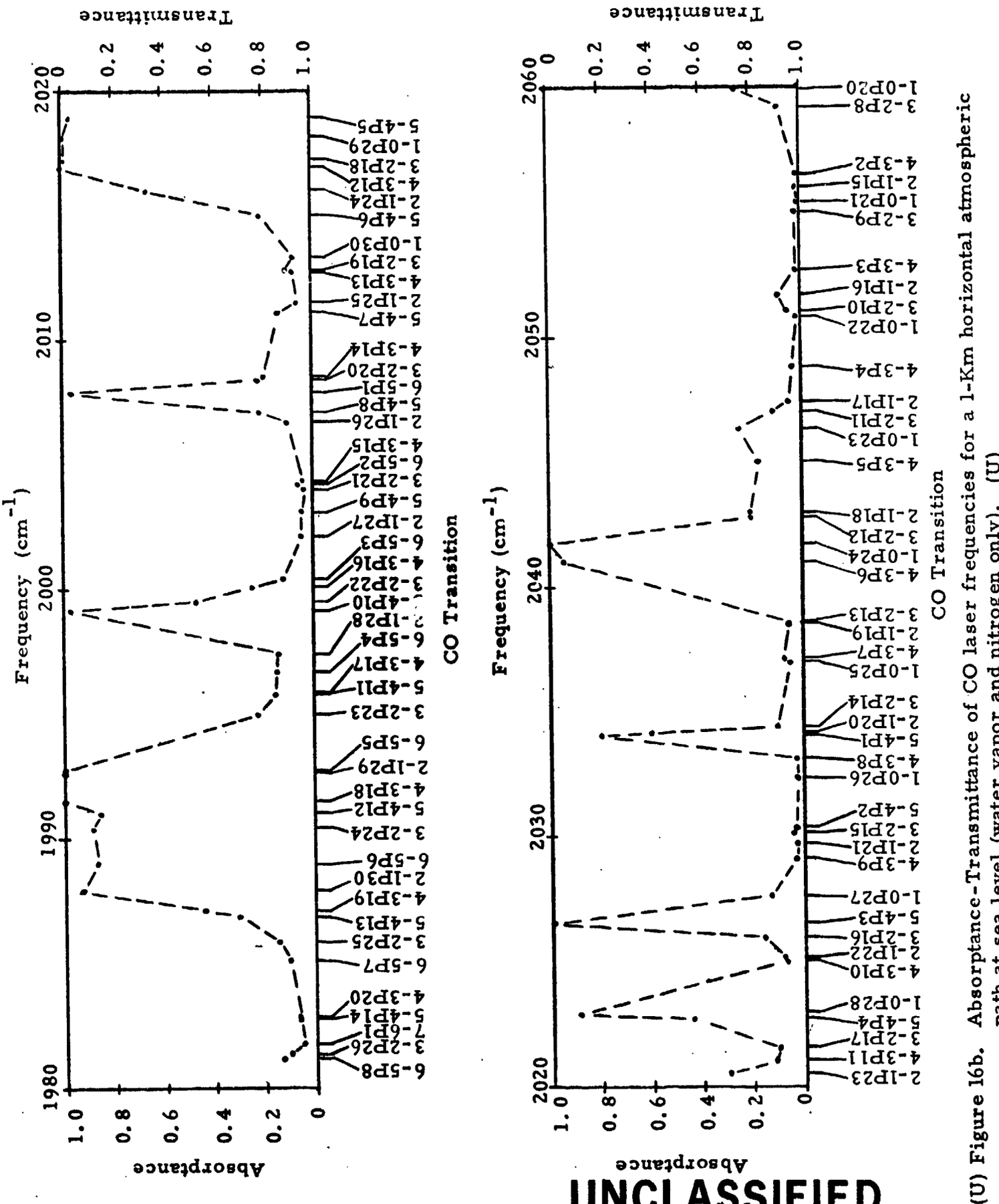

(U) Figure 16b. Absorptance-Transmittance of CO laser frequencies for a 1-Km horizontal atmospheric path at sea level (water vapor and nitrogen only). (U)

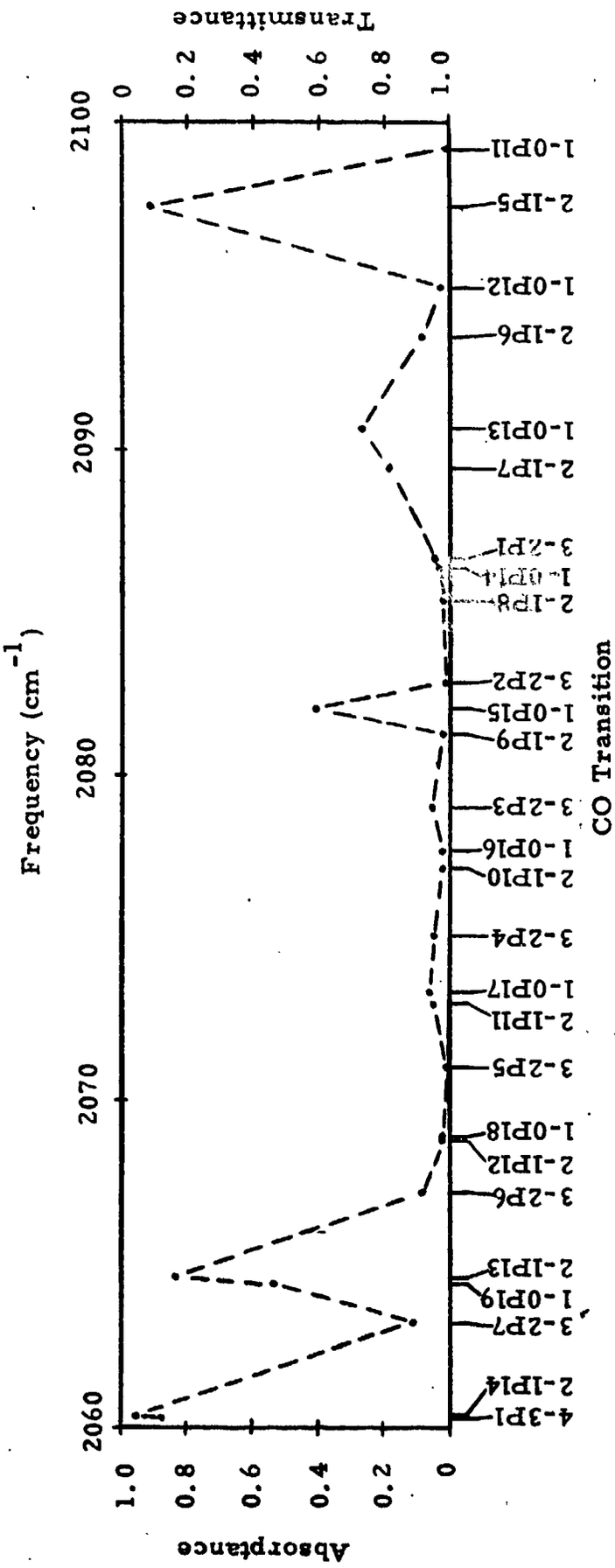

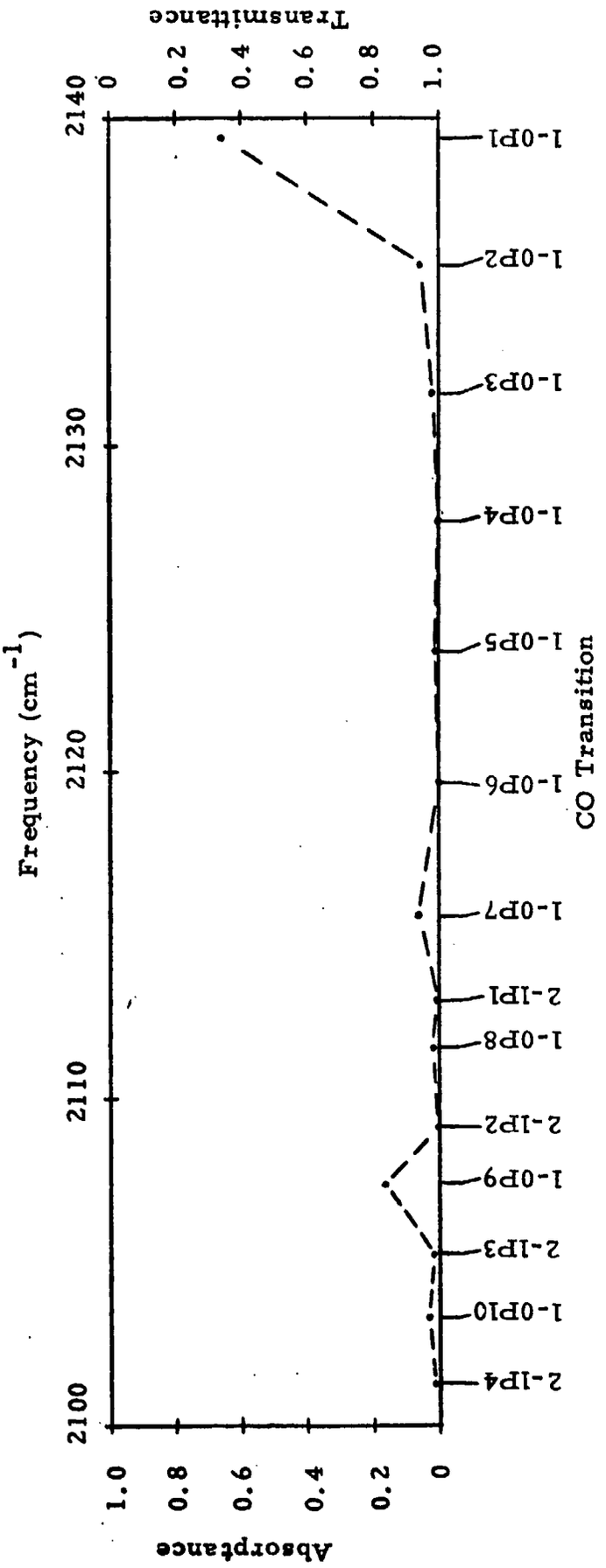

(U) Figure 16c. Absorptance-Transmittance of CO laser frequencies for a 1-Km horizontal atmospheric path at sea level (water vapor and nitrogen only). (U)

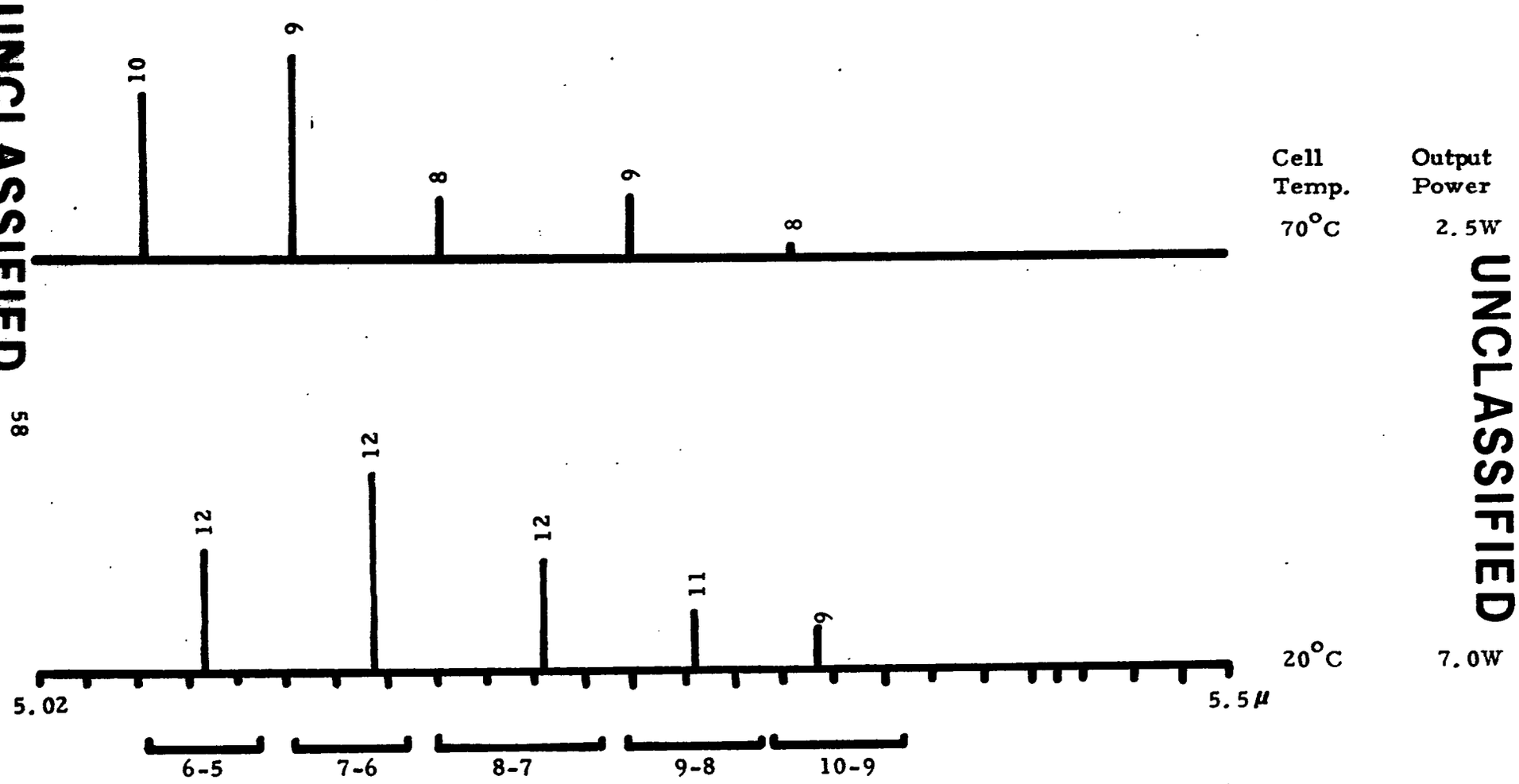

(U) Figure 17. Output spectra and power of a CO laser with an intracavity water vapor cell (output mirror reflectivity 85%; current 5 mA, laser wall temperature 77°K). (U)

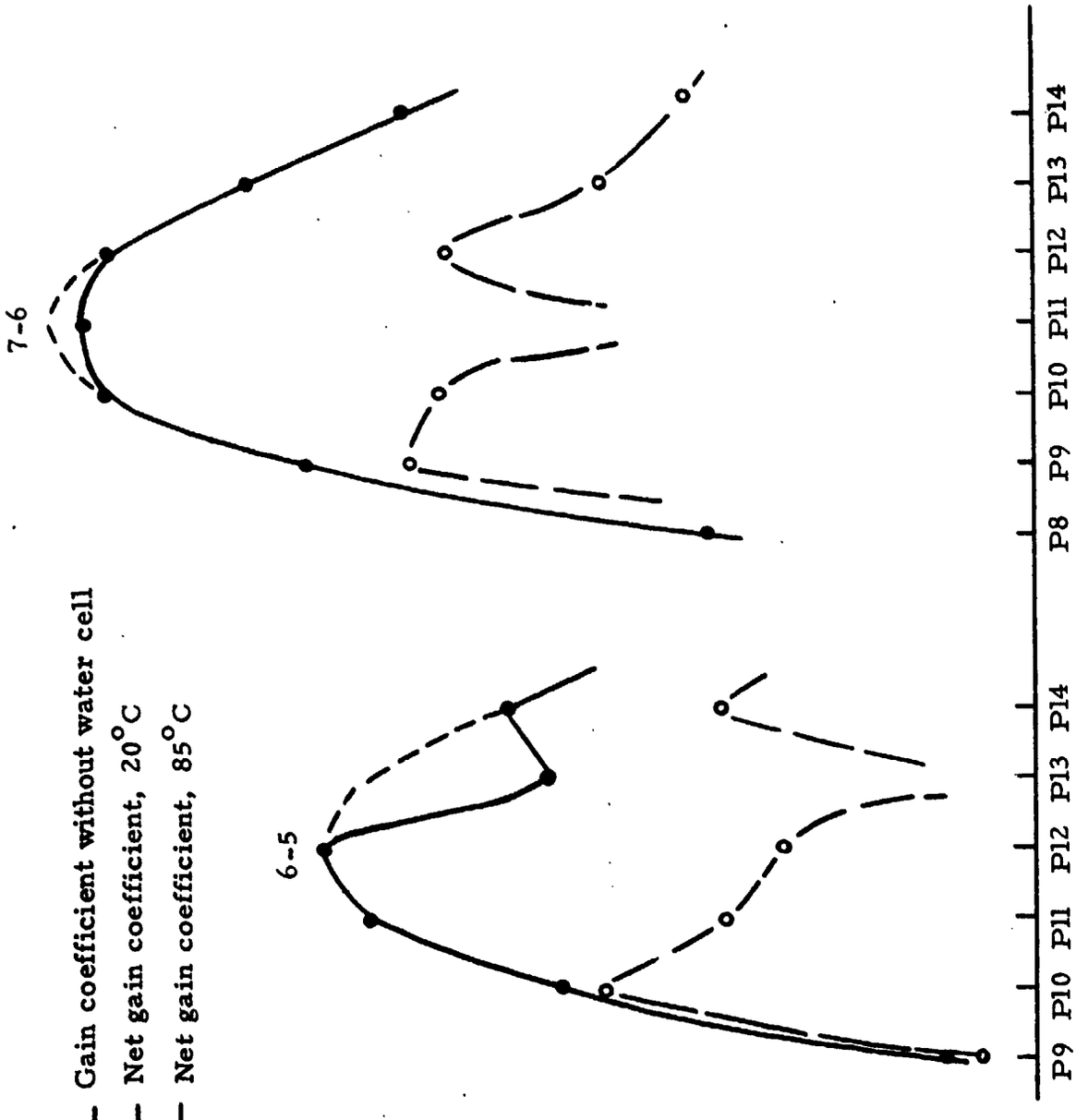

(U) Figure 18. Net single pass gain coefficients of a CO laser with an intracavity water vapor cell. (U)

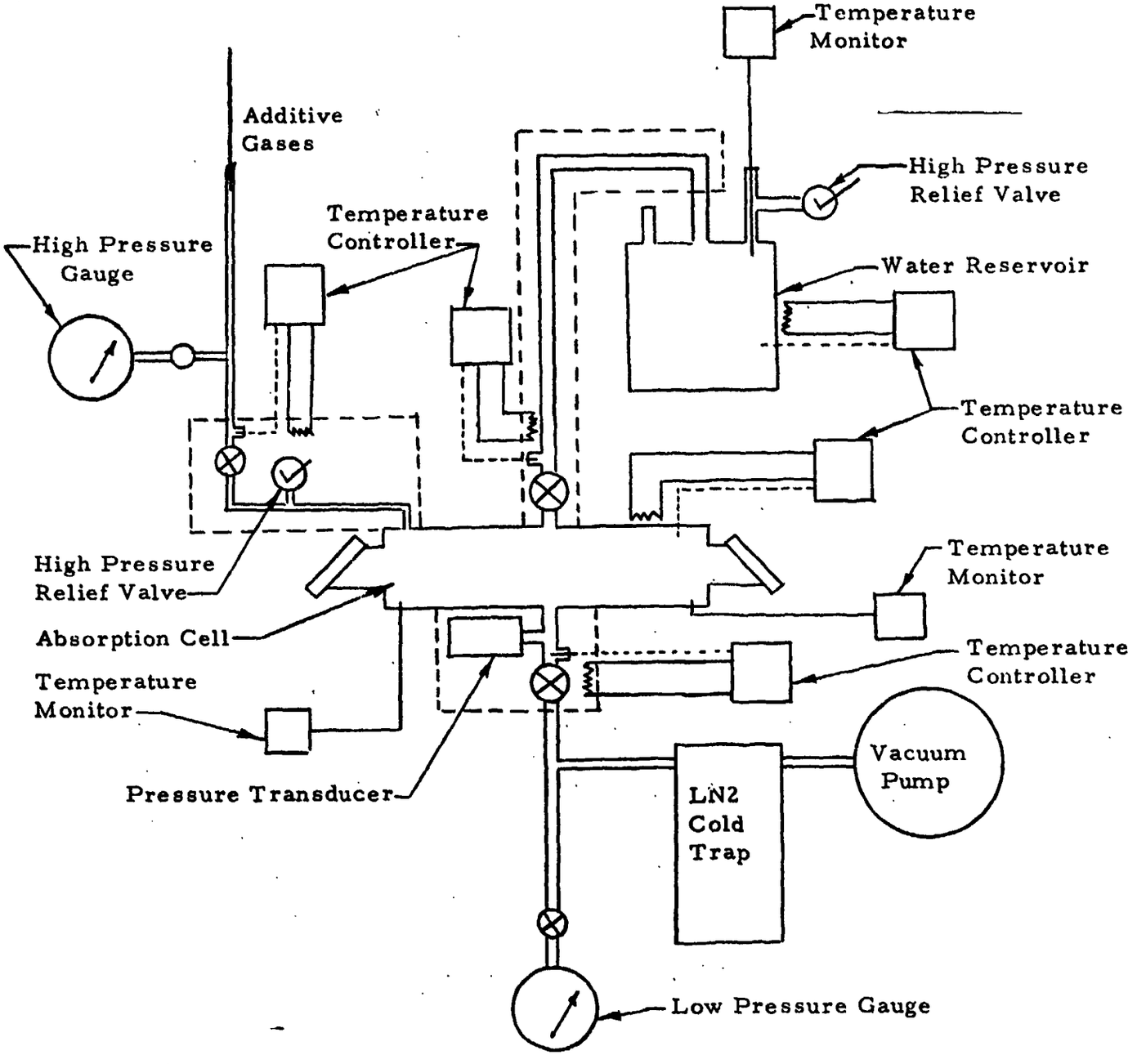

(U) Figure 19. Absorption cell system for spectral line selection studies. (U)

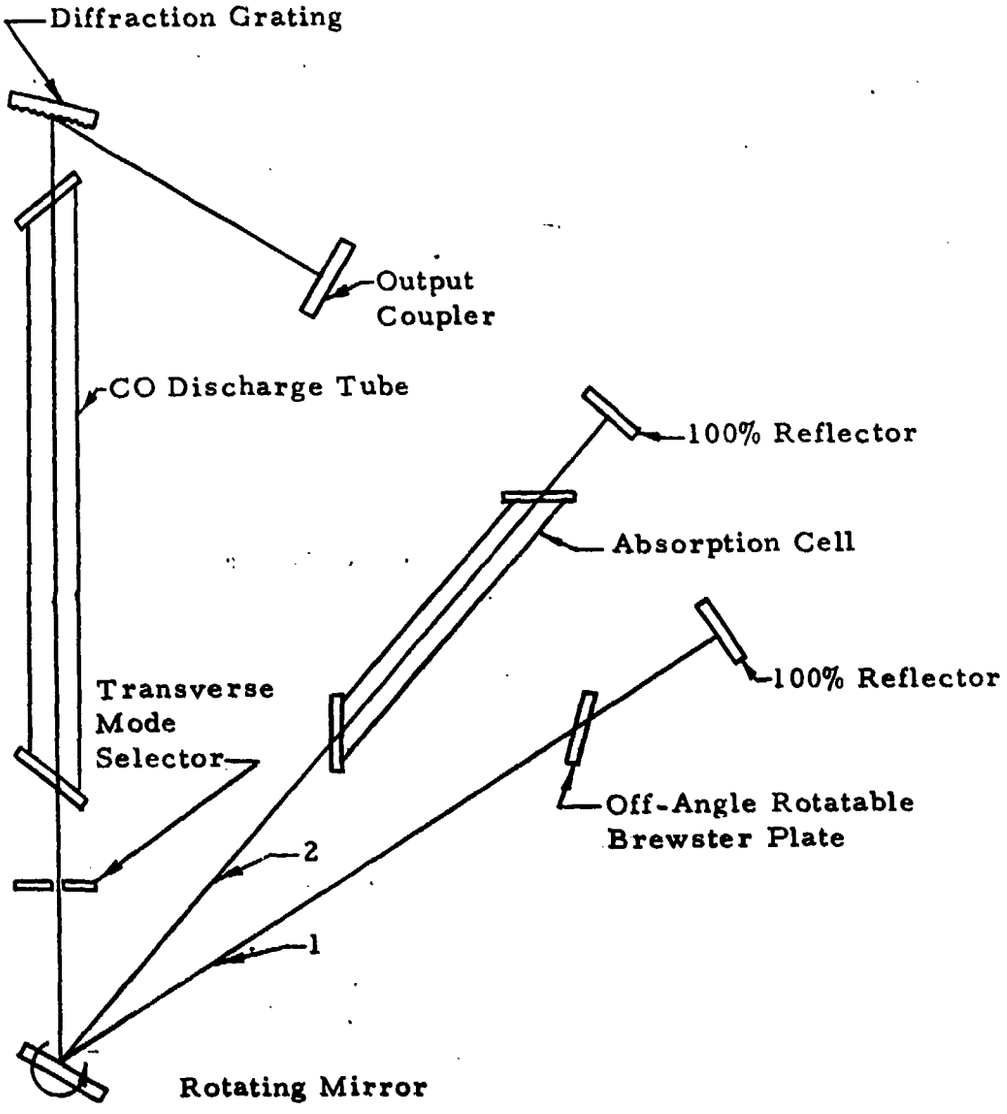

(U) Figure 20. Optical set-up for low power line selection studies. (U)

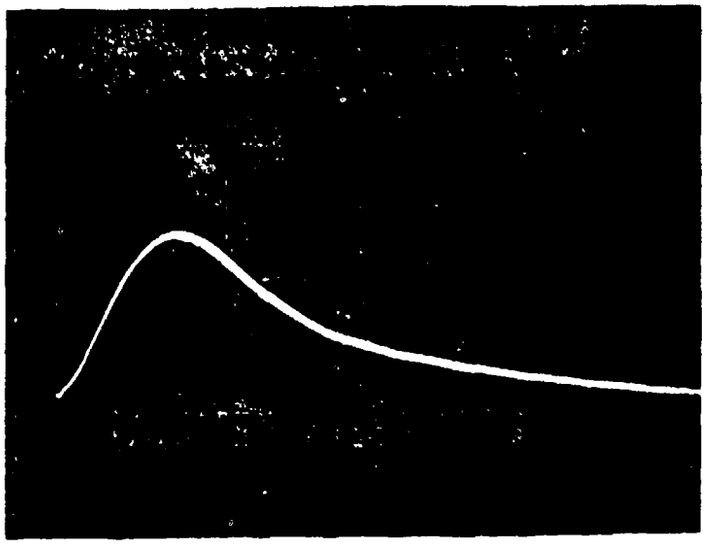

a. Vapor cell - evacuated.
Brewster plate - at Brewster's angle. (U)

b. Vapor cell - 188 torr of 68°C water vapor.
Brewster plate - at Brewster's angle. (U)

c. Vapor cell - 188 torr of 68°C water vapor.
Brewster plate - at Brewster's angle + 14.2°. (U)

(U) Figure 21. 10-9P(14) Q-switched CO laser spectrometer pulses from vapor cell and Brewster plate resonators (1 μsec/div.) (U)

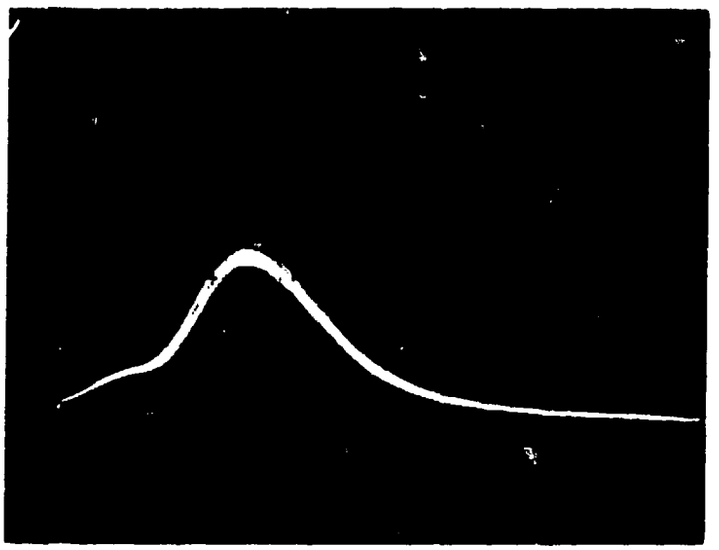

(U) Figure 22. Total output pulses of Q-switched CO laser from vapor cell and Brewster plate resonators - grating tuned for 10-9P(14) operation (1 μsec/div.) (U)

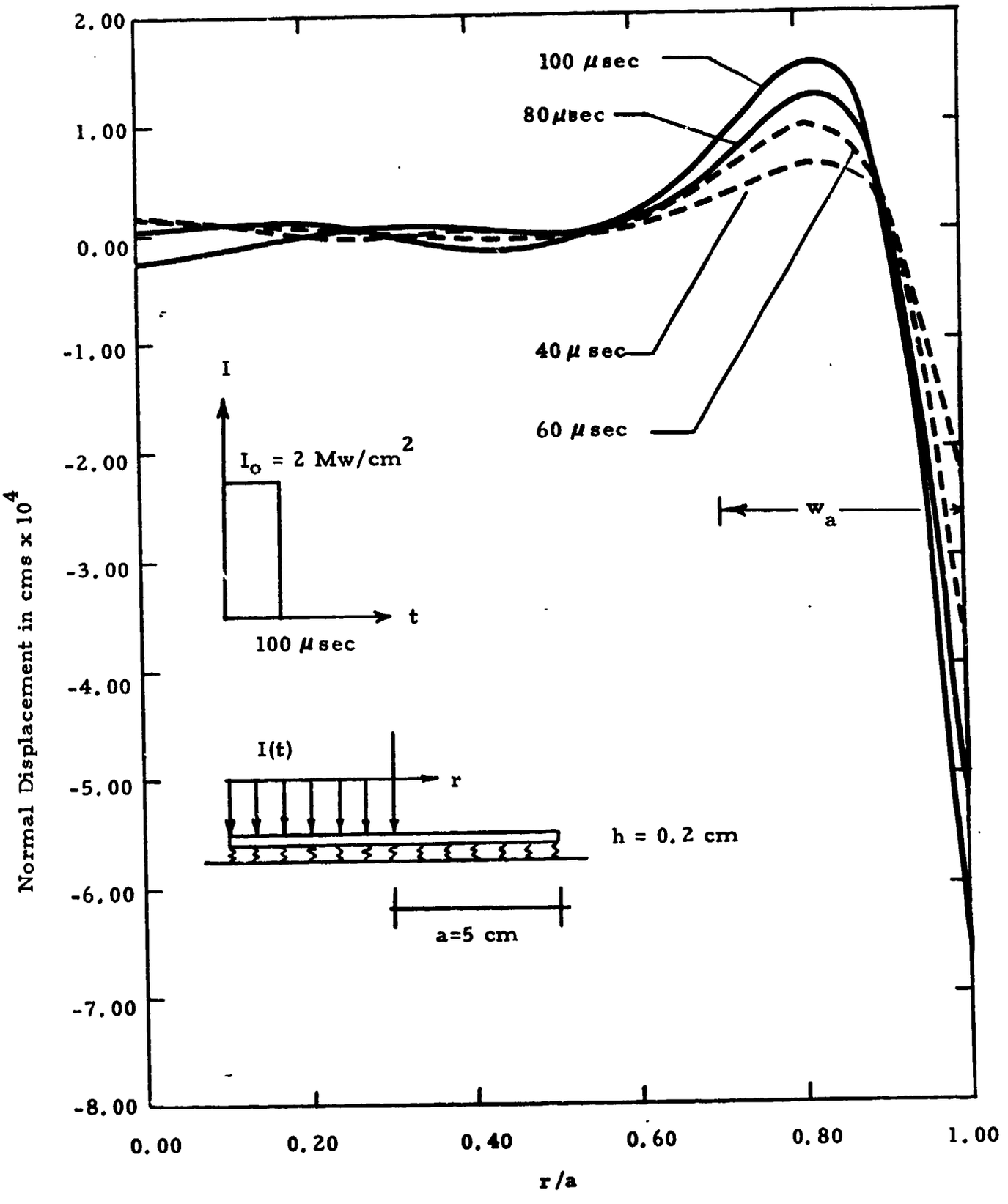

(U) Figure 23. Transient Response - Mirror Deflection (Continuous Model). (U)

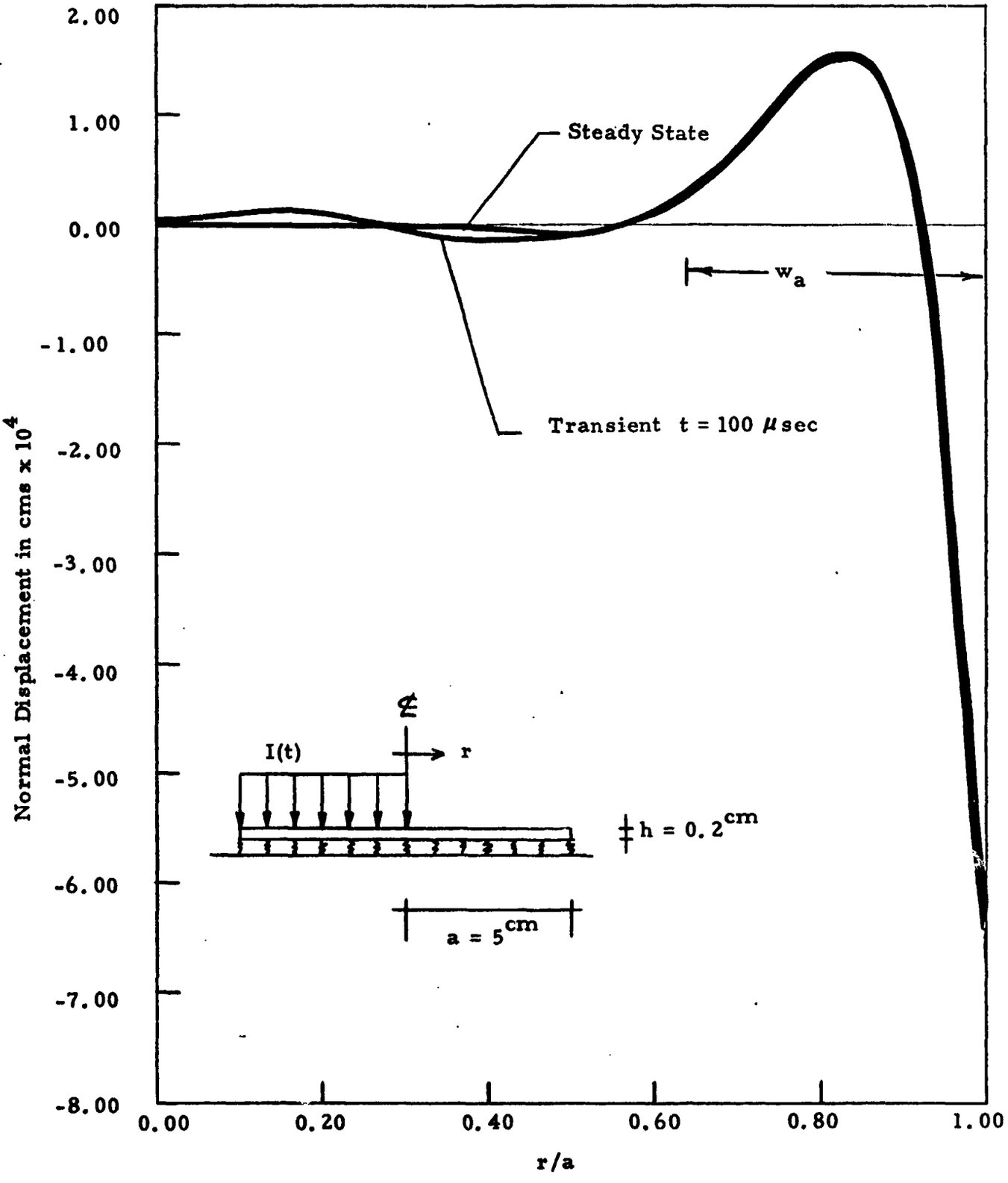

(U) Figure 24. Comparison between static and transient response (with a uniform continuous foundation assumed) (U)

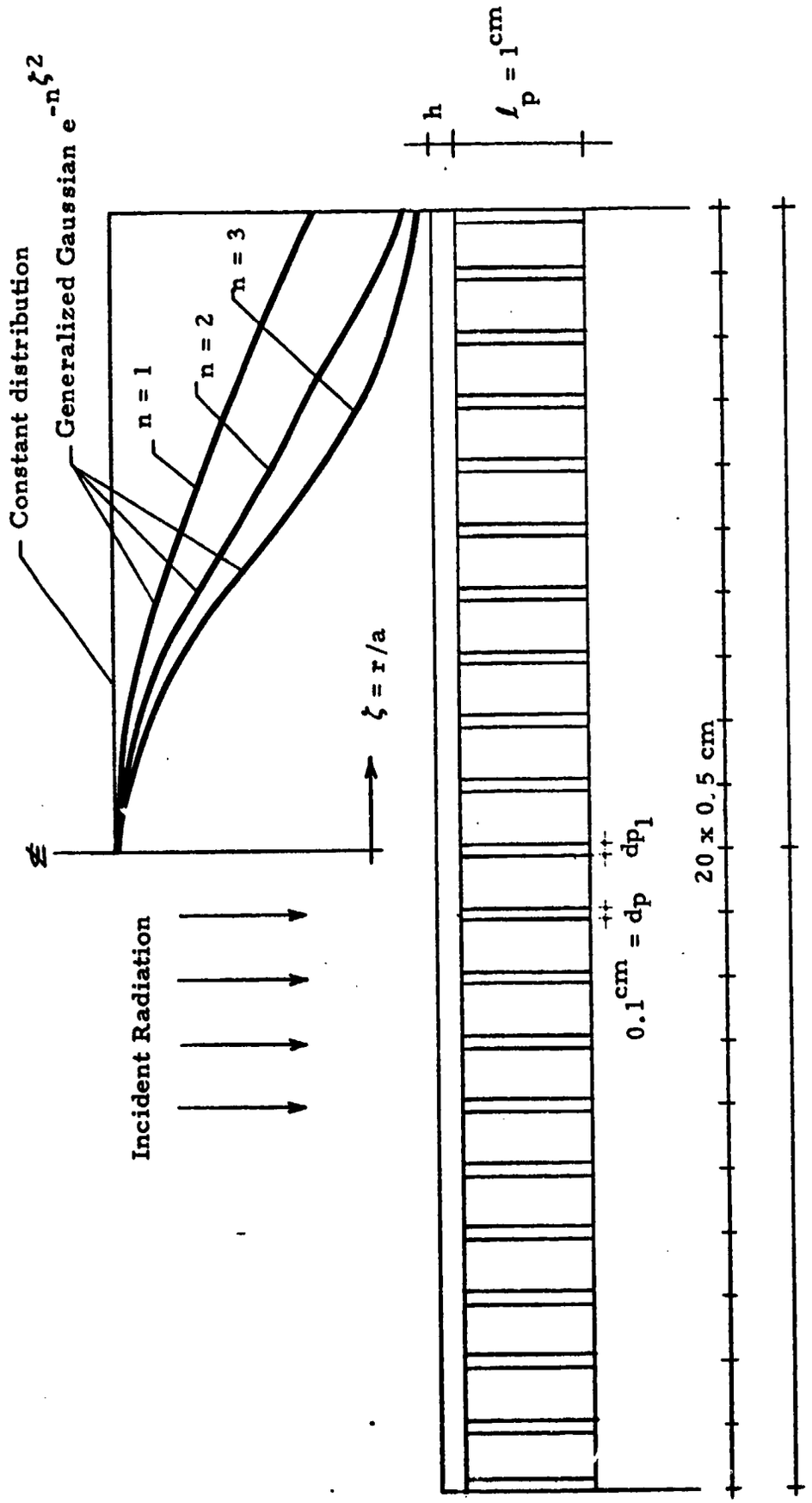

(U) Figure 25. Post-mounted faceplate cross-section and loading distributions considered. (U)

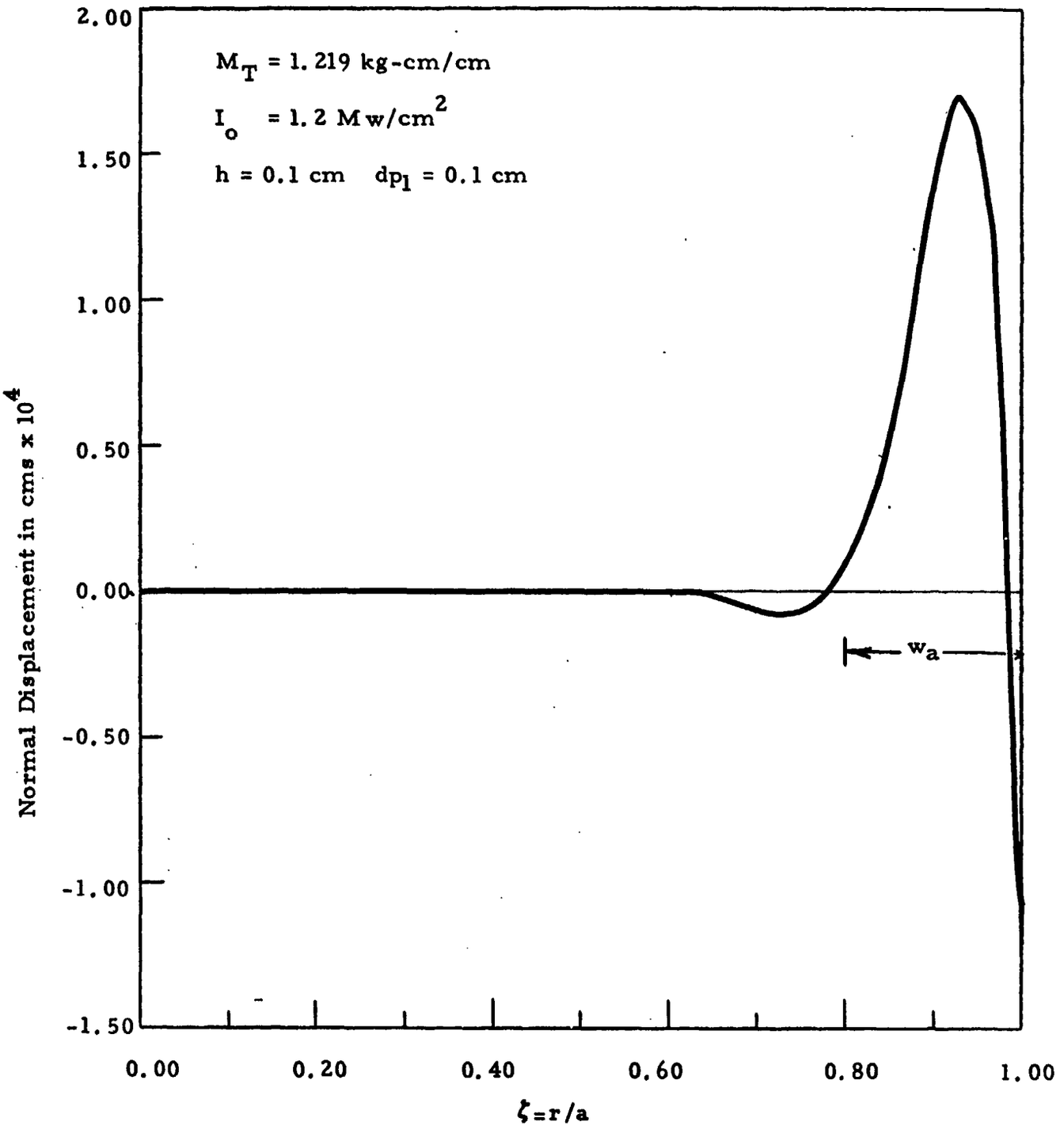

(U) Figure 26. Post-mounted mirror distortion under a uniform thermal load. (U)

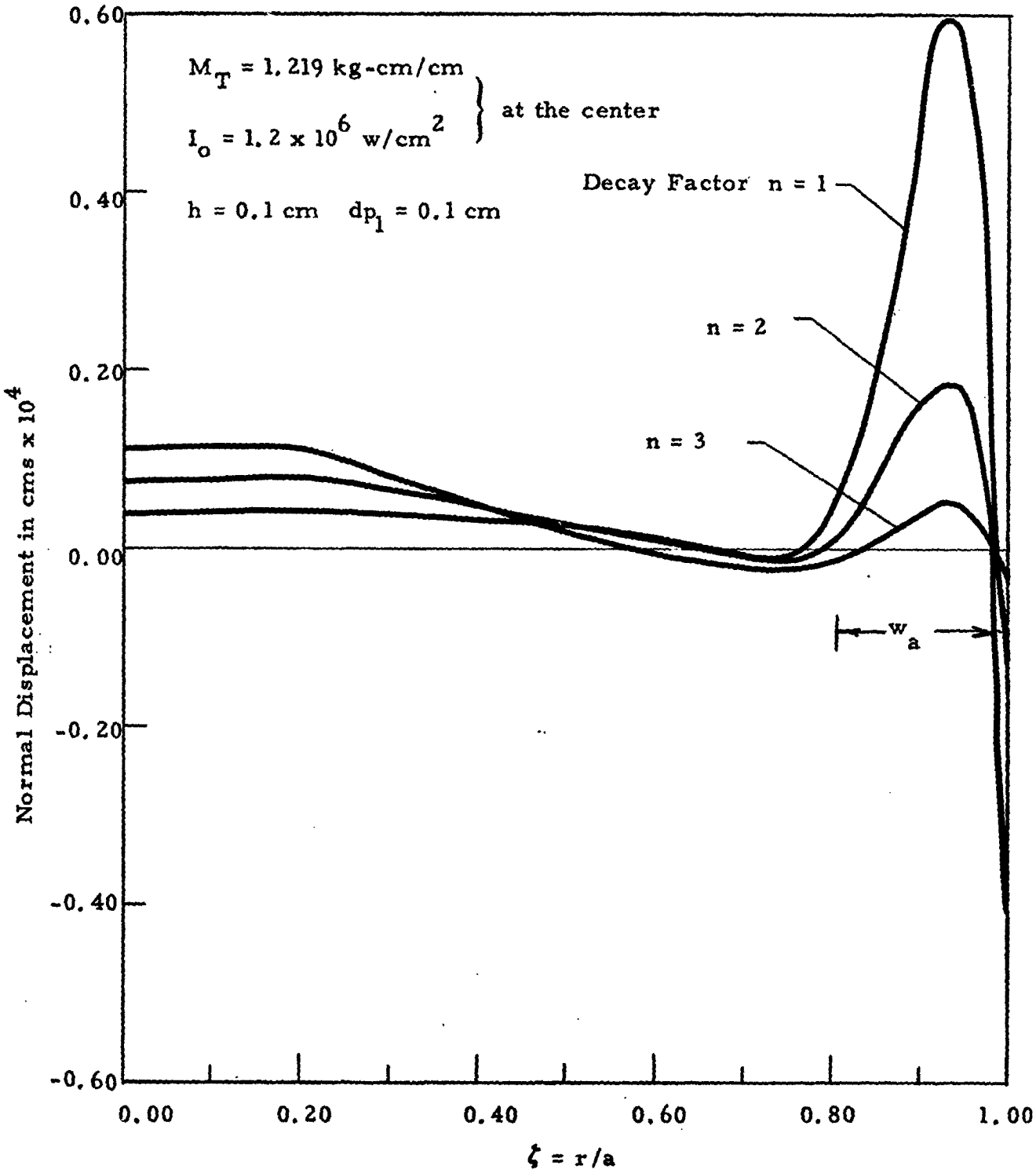

(U) Figure 27. Post-mounted mirror distortion for a generalized Guassian load distribution with n = 1, 2 and 3. (U)

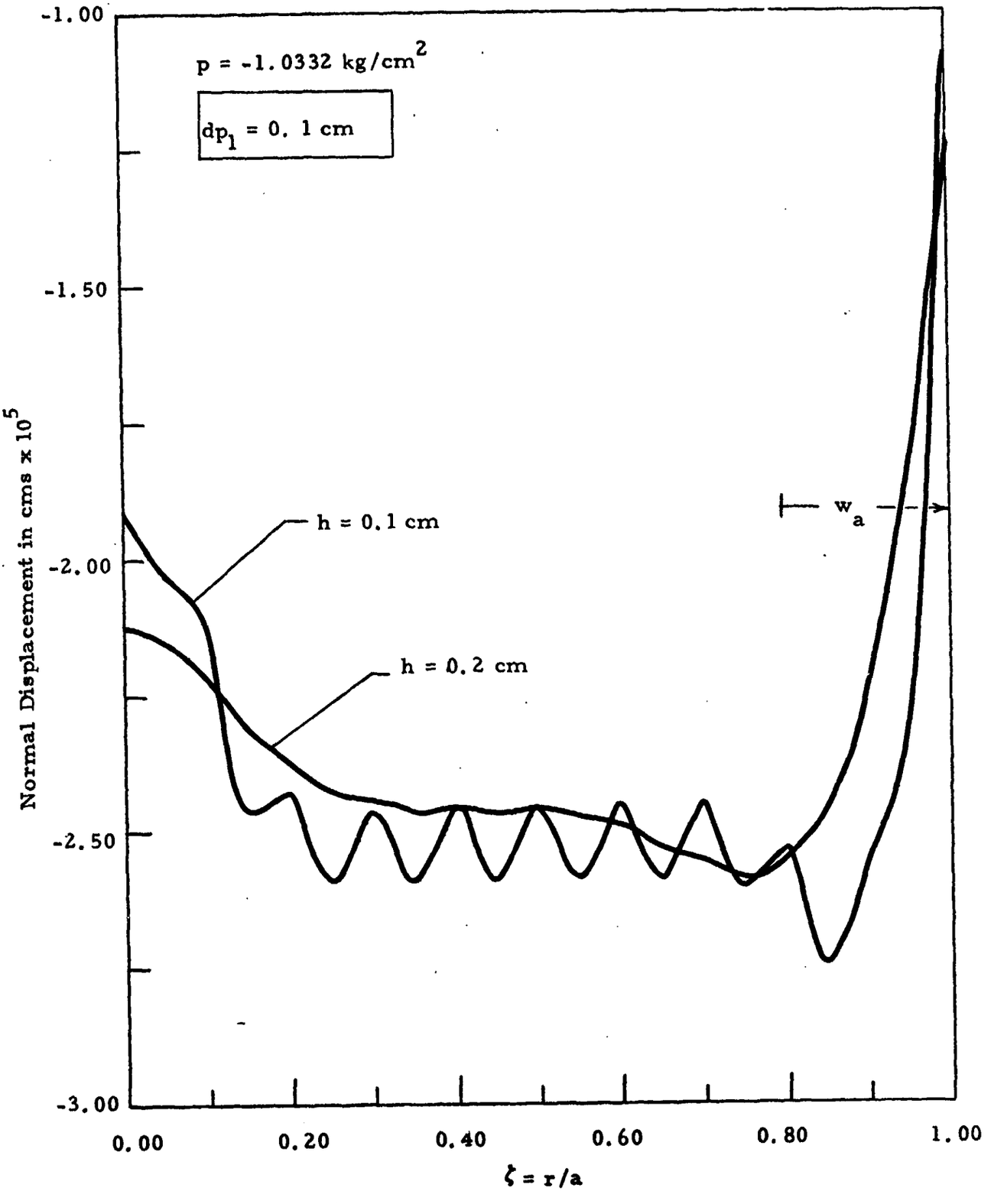

(U) Figure 28. Mirror distortion for 1 atm uniform pressure load, for a central post diameter of 0.1 cm and two thicknesses (h) of the substrate. (U)

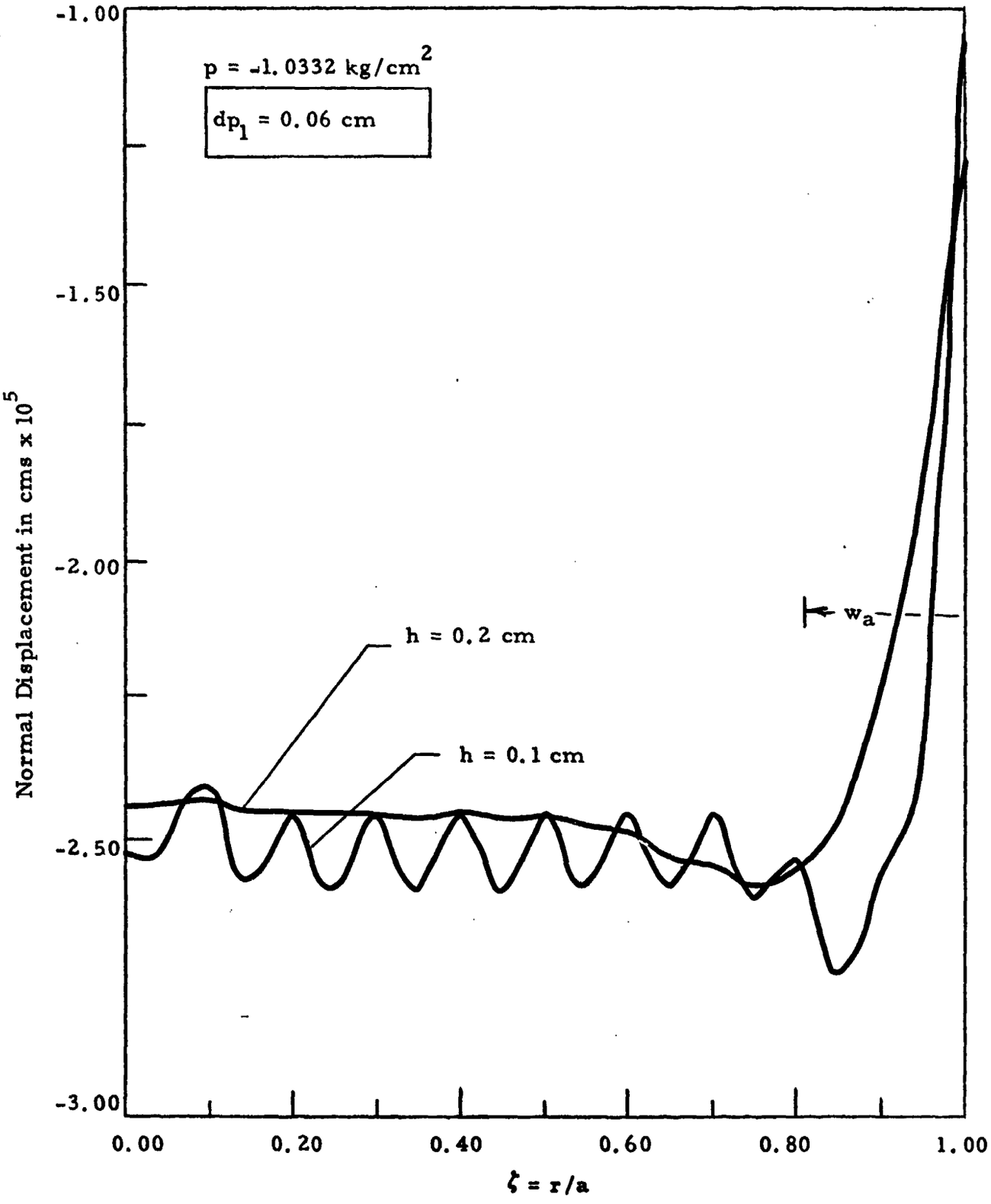

(U) Figure 29. Mirror distortion for 1 atm uniform pressure, for a central post diameter of 0.06 cm and two thicknesses (h) of the substrate. (U)

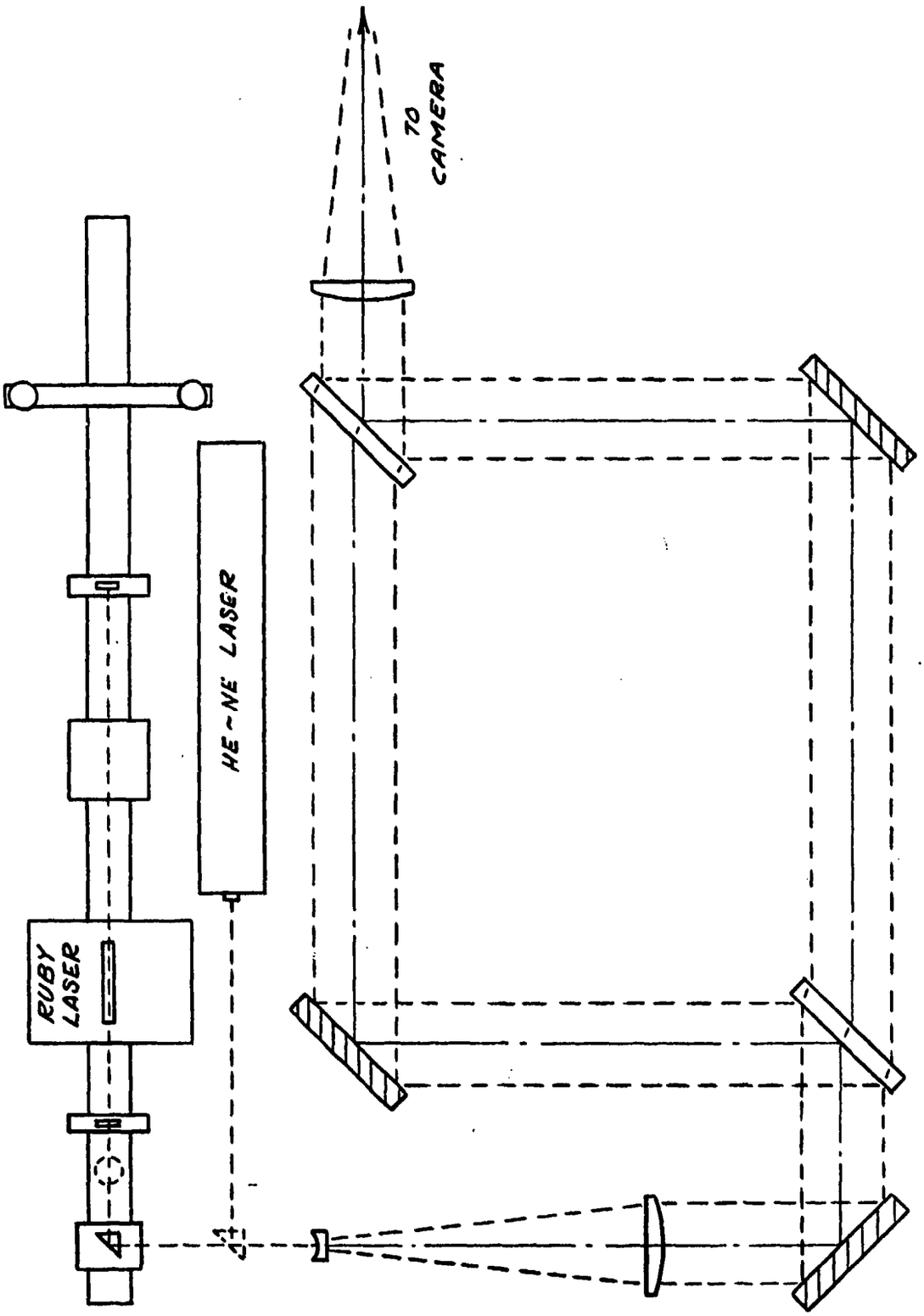

(U) Figure 30. Diagram of the interferometer facility under development. (U)

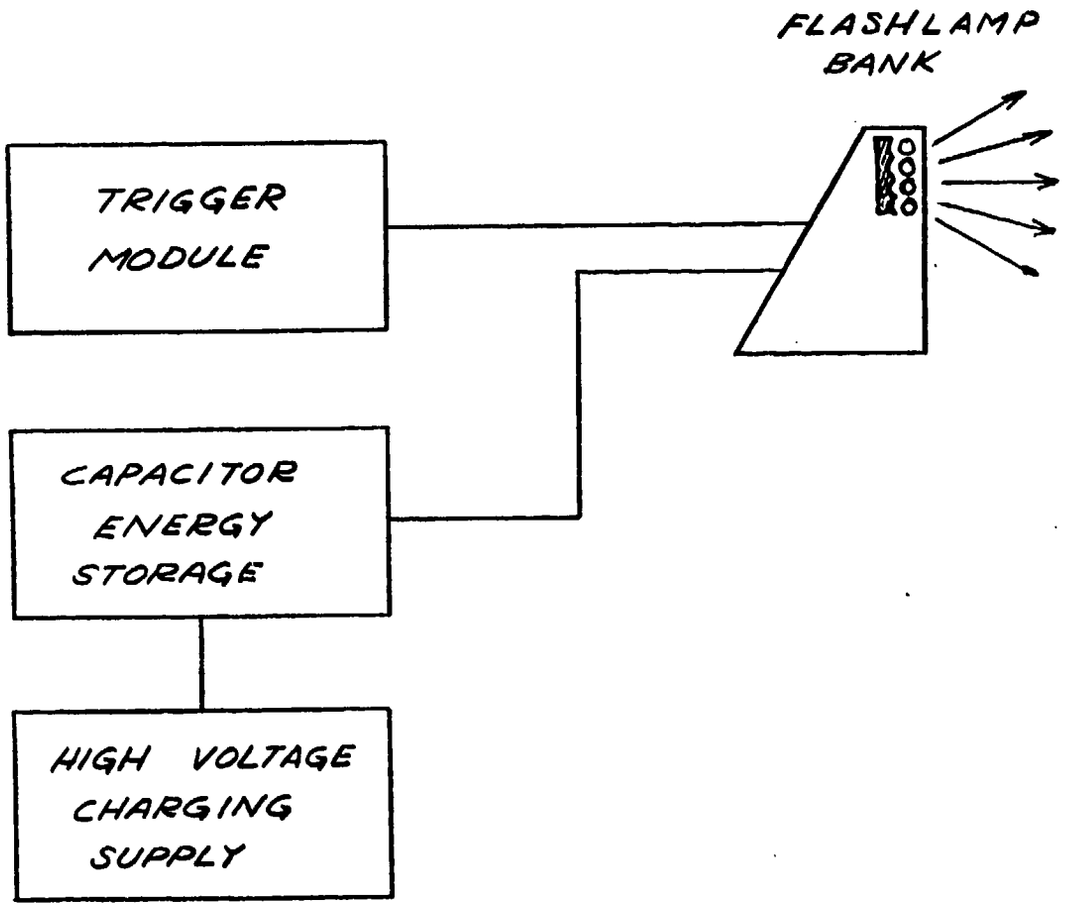

(U) Figure 31. Block diagram of the flashlamp loading system. (U)

SECRET
Security Classification

DOCUMENT CONTROL DATA - R & D

(Security classification of title, body of abstract and indexing annotation must be entered when the overall report is classified)

1. ORIGINATING ACTIVITY (Corporate author) NORTHROP CORPORATION, Research and Technology Laser Systems Department	2a. REPORT SECURITY CLASSIFICATION SECRET 2b. GROUP GROUP 3

3. REPORT TITLE

HIGH POWER CO LASER, SEMI ANNUAL REPORT (U)

4. DESCRIPTIVE NOTES (Type of report and inclusive dates)

SEMI ANNUAL - 1 AUGUST 1971 THROUGH 29 FEBRUARY 1972

5. AUTHOR(S) (First name, middle initial, last name)

NORTHROP LASER SYSTEMS DEPARTMENT

6. REPORT DATE	7a. TOTAL NO. OF PAGES	7b. NO. OF REFS
MARCH 1972	74	12

8a. CONTRACT OR GRANT NO.	9a. ORIGINATOR'S REPORT NUMBER(S)
N00014-72-C-0043 b. PROJECT NO.	NLSD 72-7R
c. d.	9b. OTHER REPORT NO(S) (Any other numbers that may be assigned this report) NONE

10. DISTRIBUTION STATEMENT

~~DISTRIBUTION OF THIS DOCUMENT IS UNLIMITED.~~

11. SUPPLEMENTARY NOTES	12. SPONSORING MILITARY ACTIVITY
NONE	ADVANCED RESEARCH PROJECTS AGENCY, ARPA ORDER NO. 1806

13. ABSTRACT

(U) The first six month effort on the High Power CO Laser Program is reviewed. The program is directed toward the development of the required CO laser technology, the required component technology and the design and construction of intermediate power laser devices. The results of analytical and experimental investigation of the basic characteristics of the laser are reviewed and initial data from a high pressure electrically excited CO laser device are discussed.

DD FORM 1 NOV 68 1473 (PAGE 1)

S/N 0101-807-6801

SECRET
Security Classification

14. KEY WORDS	LINK A		LINK B		LINK C	
	ROLE	WT	ROLE	WT	ROLE	WT
CO Laser						
Molecular Lasers						
Electric Discharge Lasers						
High Power Lasers						

DEPARTMENT OF THE NAVY
OFFICE OF NAVAL RESEARCH
800 NORTH QUINCY STREET
ARLINGTON, VA 22217-5660

IN REPLY REFER TO

5510/1
Ser 93/804
26 Aug 98

From: Chief of Naval Research
To: Defense Technical Information Center
ATTN: Bill Bush, DTIC-OCQ
8725 John J. Kingman Road Suite 0944
Ft. Belvoir, VA 22060-6218

Subj: DECLASSIFICATION OF ONR DOCUMENTS

1. The following documents have been declassified by authority of the Chief of Naval Research and assigned Distribution Statement A:

AD 518 509
AD 520 202
AD 522 005

2. Questions may be directed to the undersigned on (703) 696-4619.

Peggy Lambert

PEGGY LAMBERT
By direction